Aus der Klinik für Augenheilkunde
Direktor: Prof. Dr. med. Walter Sekundo

des Fachbereichs Medizin der Philipps-Universität Marburg

Titel der Dissertation

Topographic analysis of the centration of the treatment zone after Small Incision Lenticule Extraction (SMILE) surgery for myopia and myopic astigmatism and comparison to Femtosecond laser-assisted LASIK (FS-LASIK)

Inaugural-Dissertation zur Erlangung des Doktorgrades der gesamten Humanmedizin
dem Fachbereich Medizin der Philipps-Universität Marburg

vorgelegt von
Apostolos Lazaridis
aus Thessaloniki, Griechenland
Marburg, 2018

Angenommen vom Fachbereich Medizin der Philipps-Universität Marburg
am: 14.11.2018

Gedruckt mit Genehmigung des Fachbereichs

Dekan: Herr Prof. Dr. Helmut Schäfer

Referent: Herr Prof. Dr. med. Walter Sekundo

Korreferent: Herr Priv. Doz. Dr. med. Suphi Taneri

Dedicated to Stavroula, the love and inspiration of my life.

Table of Contents **Page**

List of abbreviations

BL	Bowman's layer
CA	corneal apex
CDVA	corrected distance visual acuity
CSCLR	coaxially sighted corneal light reflex
D	dioptre
DM	Descemet's membrane
EPC	entrance pupil centre
FLEx	Femtosecond Lenticule Extraction
FS-LASIK	Femtosecond laser-assisted Laser-assisted in Situ Keratomileusis
HOA	higher order aberrations
LASIK	Laser-assisted in Situ Keratomileusis
LESC	limbal epithelial stem cell
UDVA	uncorrected distance visual acuity
OD	right eye
OS	left eye
PMPD	point of maximum pachymetric difference
ReLEx	Refractive Lenticule Extraction
SEQ	spherical equivalent
SMILE	Small Incision Lenticule Extraction
TAC	transient amplifying cell

Abstract

Introduction

Corneal refractive surgery reshapes the cornea in order to change its refractive power and correct refractive errors such as myopia, hyperopia and astigmatism. An important factor associated with the postoperative quality of vision is the centration of the treatment zone. A treatment zone that is decentered in relation to the visual axis may affect the functional corneal morphology and therefore the quality of the visual outcome after the treatment. Functional deficits, such as reduced corrected distance and near visual acuity, irregular astigmatism, halos, glare, reduced contrast sensitivity and monocular diplopia are associated with decentered treatment zones, even in cases of subclinical decentration (<1.0 mm).

Purpose

An argument often expressed by refractive surgeons is that in small incision lenticule extraction (SMILE) a precise centration cannot be guaranteed due to the subjective intraoperative alignment and lack of eye tracking. Therefore, the purpose of this study is to investigate and compare the centration of the treatment zone between eyes treated with SMILE and active eye-tracker assisted femtosecond laser-assisted LASIK (FS-LASIK), and evaluate the pattern of the achieved centration.

Methods

In the present retrospective study, 69 myopic eyes of 36 patients who underwent SMILE were compared to 69 myopic eyes of 36 patients treated with FS-LASIK. All procedures were performed at the Department of Ophthalmology, Philipps University of Marburg, by a single surgeon using the VisuMax® femtosecond-laser and MEL-80® excimer-laser (Carl Zeiss Meditec AG, Jena, Germany). Pentacam™ (Oculus

Optikgeräte GmbH, Wetzlar, Germany) was used for preoperative and 3-month postoperative topography and pachymetry. The centration of the treatment zone was estimated by the distance of the point of the maximum pachymetric difference (PMPD) on the corneal thickness differential map from the coaxially sighted corneal light reflex (CSCLR; reference point of centration of the treatment zone in SMILE) and the topographic centre of the entrance pupil (EPC; reference point of centration of the treatment zone in FS-LASIK). The distribution of angle K (angular distance between visual and pupillary axis) was assessed preoperatively in both groups by depicting the exact location of the CSCLR in relation to the EPC. The pattern of the achieved centration was evaluated by depicting on a Cartesian plane the location of the PMPD in relation to the EPC. The pattern of the achieved centration was compared to the preoperative pattern of angle K (pattern of the preoperative CSCLR in relation to the EPC).

Results

In SMILE group, the mean decentration of the treatment zone from the EPC was 0.326 ± 0.196 mm, ranging from 0.014 to 1.062 mm, whereas the centration of the treatment zone demonstrated a nasalization pattern. In FS-LASIK group, the mean decentration of the treatment zone from the EPC was 0.452 ± 0.224 mm, ranging from 0.02 to 1.040 mm, whereas the centration of the treatment zone demonstrated a random pattern. In relation to the CSCLR, the decentration in SMILE was 0.315 ± 0.211 mm, ranging from 0.0 to 1.131 mm, whereas FS-LASIK eyes demonstrated a mean decentration of 0.516 ± 0.254 mm, ranging from 0.103 to 1.265 mm. The decentration from the reference point of its technique (CSCLR in SMILE; EPC in FS-LASIK) was significantly more extended in FS-LASIK group ($P < 0.001$).

The evaluation of angle K based on the location of the preoperative CSCLR in relation to the EPC showed in SMILE group 32 right eyes and 24 left eyes with positive angle K, 2 right eyes and 11 left eyes with negative angle K, and no eyes with 0° angle K. In FS-LASIK group, there were 29 right eyes and 22 left eyes with positive angle K,

3 right eyes and 14 left eyes with negative angle K, and 1 right eye with 0° angle K. In both groups, the location of the preoperative CSCLR demonstrated a nasalization pattern. In SMILE group, the mean distance of the point corresponding to the preoperative CSCLR from the EPC was 0.227 ± 0.121 mm, ranging from 0.014 to 0.602 mm, and in FS-LASIK group was 0.206 ± 0.097 mm, ranging from 0.045 to 0.457 mm. Statistical analysis showed no significant difference between the two groups ($P = 0.201$). After SMILE, the achieved centration followed the preoperative pattern of angle K in 52 out of 69 eyes (75.36%), whereas only 32 of 69 eyes (46.37%) followed that pattern after FS-LASIK ($P < 0.001$).

Conclusions

The centration of the treatment zone as evaluated on corneal thickness differential maps was better for patient-controlled fixation during SMILE compared to active eye tracker-assisted FS-LASIK. Moreover, the results suggest that centring the refractive procedure on the CSCLR (as in SMILE), results in a more natural outcome, which follows the preoperative pattern of angle K as opposed to centring the refractive procedure on the EPC (as in FS-LASIK).

Zusammenfassung

Einleitung

Die refraktive Chirurgie der Hornhaut formt die Hornhaut neu, um ihre Brechkraft zu ändern und Refraktionsfehler wie Kurzsichtigkeit, Weitsichtigkeit und Astigmatismus zu korrigieren. Ein wichtiger Faktor, der mit der postoperativen Qualität des Sehens verbunden ist, ist die Zentrierung der Behandlungszone. Eine Behandlungszone, die in Bezug auf die Sehachse dezentriert ist, kann die funktionelle Hornhautmorphologie und damit die Qualität des visuellen Ergebnisses nach der Behandlung beeinflussen. Funktionelle Defizite, wie verminderte korrigierte Fern- und Nahvisus, irregulärer Astigmatismus, Halos, Blendung, verminderte Kontrastempfindlichkeit und monokulare Diplopie, sind mit dezentrierten Behandlungszonen verbunden, auch bei subklinischer Dezentrierung (<1,0 mm).

Zweck

Ein häufig von refraktiven Chirurgen geäußertes Argument ist, dass bei Small Incision Lenticule Extraction (SMILE) eine genaue Zentrierung aufgrund der subjektiven intraoperativen Ausrichtung und des Fehlens eines Eye-Trackers nicht garantiert werden kann. Ziel dieser Studie ist es daher, die Zentrierung der Behandlungszone zwischen den mit SMILE behandelten und mit aktiver Eye-Tracker-assistierten Femtosekunden-Laser-assistierten LASIK (FS-LASIK) behandelten Augen zu untersuchen und zu vergleichen und das Muster der erreichten Zentrierung zu bewerten.

Methoden

In der vorliegenden retrospektiven Studie wurden 69 myopische Augen von 36 Patienten, die SMILE erhielten, mit 69 myopen Augen von 36 Patienten, die mit FS-LASIK behandelt wurden, verglichen. Alle Verfahren wurden an der Augenklinik der Philipps-Universität Marburg von einem einzigen Chirurgen mit dem VisuMax®

Femtosekunden-Laser und MEL-80® Excimer-Laser (Carl Zeiss Meditec AG, Jena, Deutschland) durchgeführt. Pentacam™ (Oculus Optikgeräte GmbH, Wetzlar, Deutschland) wurde für die präoperative und 3-monatige postoperative Topographie und Pachymetrie eingesetzt. Die Zentrierung der Behandlungszone wurde durch den Abstand des Punktes der maximalen pachymetrischen Differenz (maximum pachymetric difference (PMPD)) auf der differentiellen Karte der Hornhautdicke vom koaxial gesichteten Hornhautreflex (coaxially sighted corneal light reflex (CSCLR); Bezugspunkt der Zentrierung der Behandlungszone in SMILE) und das topographische Zentrum der Eintrittspupille (entrance pupil centre (EPC); Bezugspunkt der Zentrierung der Behandlungszone bei FS-LASIK) geschätzt. Die Verteilung des Winkels K (Winkelabstand zwischen visueller und Pupillenachse) wurde in beiden Gruppen präoperativ beurteilt, indem der genaue Ort des CSCLR in Relation zum EPC dargestellt wurde. Das Muster der erzielten Zentrierung wurde bewertet, indem auf einer kartesischen Ebene der Ort des PMPD in Bezug auf den EPC dargestellt wurde. Das Muster der erreichten Zentrierung wurde mit dem präoperativen Muster des Winkels K (Muster des präoperativen CSCLR in Bezug auf den EPC) verglichen.

Ergebnisse

In der SMILE-Gruppe betrug die mittlere Dezentrierung der Behandlungszone aus dem EPC 0,326 ± 0,196 mm und reichte von 0,014 bis 1,062 mm, während die Zentrierung der Behandlungszone ein Nasalisierungsmuster zeigte. In der FS-LASIK-Gruppe betrug die mittlere Dezentrierung der Behandlungszone aus dem EPC 0,452 ± 0,224 mm, im Bereich von 0,02 bis 1,040 mm, während die Zentrierung der Behandlungszone ein zufälliges Muster zeigte. In Bezug auf die CSCLR betrug die Dezentrierung in SMILE 0,315 ± 0,211 mm und reichte von 0,0 bis 1,131 mm, während FS-LASIK-Augen eine mittlere Dezentration von 0,516 ± 0,254 mm im Bereich von 0,103 bis 1,265 mm aufwiesen. Die Dezentration vom Referenzpunkt jeder Technik (CSCLR in SMILE; EPC in FS-LASIK) war in der FS-LASIK-Gruppe signifikant ausgedehnter ($P < 0{,}001$). Die Auswertung des Winkels K basierend auf dem Ort der präoperativen CSCLR in Relation zum EPC zeigte in der SMILE Gruppe 32 rechte Augen und 24 linke Augen

mit positivem Winkel K, 2 rechte Augen und 11 linke Augen mit negativem Winkel K und keine Augen mit 0 ° Winkel K. In der FS-LASIK Gruppe gab es 29 rechte Augen und 22 linke Augen mit positivem Winkel K, 3 rechte Augen und 14 linke Augen mit negativem Winkel K und 1 rechtes Auge mit 0 ° Winkel K. In beiden Gruppen , der Ort der präoperativen CSCLR zeigte ein Nasalisierungsmuster. In der SMILE Gruppe betrug der mittlere Abstand des Punktes, der dem präoperativen CSCLR aus dem EPC entsprach, 0,227 ± 0,121 mm mit Reichweite von 0,014 bis 0,602 mm und in der FS-LASIK-Gruppe 0,206 ± 0,097 mm mit Reichweite von 0,045 bis 0,457 mm. Die statistische Analyse zeigte keinen signifikanten Unterschied zwischen den beiden Gruppen (P = 0,201). Nach SMILE folgte die erreichte Zentrierung dem präoperativen Muster des Winkels K in 52 von 69 Augen (75,36%), während nur 32 von 69 Augen (46,37%) diesem Muster nach FS-LASIK folgten (P <0,001).

Schlussfolgerungen

Die Zentrierung der Behandlungszone, wie sie auf differentiellen Karten der Hornhautdicke ausgewertet wurde, war besser für die patientenkontrollierte Fixierung während SMILE im Vergleich zu aktiver Eye-Tracker-assistierter FS-LASIK. Darüber hinaus legen die Ergebnisse nahe, dass eine Zentrierung der refraktiven Prozedur auf der CSCLR (wie in SMILE) zu einem natürlicheren Ergebnis führt, das dem präoperativen Muster des Winkels K folgt, im Gegensatz zur Zentrierung der refraktiven Prozedur auf der EPC (wie in FS-LASIK).

Introduction

1.0 Basic Corneal Principles: Anatomy and Physiology

Corneal Structure

The cornea is a unique transparent and avascular tissue. These features enable its optical properties. The dimensions of the cornea of an adult human are approximately 12 mm horizontally and 11.5 mm vertically. Its oval shape is due to superior and inferior scleralization. The corneal thickness is approximately 550 μm at its centre and it gradually increases towards the periphery, reaching approximately 1200 μm at the limbus (limit between cornea and sclera). Corneal thickness is associated with corneal hydration and increases with increasing hydration and slightly with age. This variance of thickness from the centre to the periphery causes the difference in the curvature of the anterior and posterior corneal surface. The anterior corneal surface is convex and aspherotorical with a central ellipsoidal 'apical cap'. This central 3 mm optical zone is almost spheric with a nearly constant curvature (radius of curvature approximately 7.5 to 8 mm). Towards its periphery, the cornea becomes flatter. The concave posterior corneal surface has a shorter radius of curvature (approximately 6.5 mm). Corneal curvature changes after birth. It is more spherical during childhood and becomes more curved horizontally in adolescence (with the rule astigmatism; horizontal curvature > vertical curvature; steeper vertical meridian) like a 'rugby ball' lying on its side. [35, 81, 82]

Innervation

The cornea has a very dense innervation. It is actually one the most densely innervated and sensitive tissues of the human body. The corneal sensory nerves derive from the ciliary nerves of the ophthalmic branch of the trigeminal nerve. The ciliary branches of the ophthalmic nerve form a perilimbal nerve ring. Nerve fibres penetrate the cornea radially in the deep peripheral stroma, lose their myelination within a short

distance from their entry point and form a subepithelial nerve plexus. After they penetrate Bowman's layer, they terminate at the wing cell level of the epithelium. This superficial innervation causes the severe pain in case of an epithelium trauma due to the exposure of the nerve endings [81, 82].

Metabolism

For the cornea's cellular metabolic activities (mainly of the epithelium and endothelium) a constant supply of ATP (from the metabolic breakdown of glucose) and oxygen is required. The glucose is supplied by diffusion from the aqueous humour. The oxygen is supplied to the cornea by diffusion from the air, through the tear fluid. The tear fluid also provides some nutrients to the underlying cornea. Moreover, the peripheral cornea receives additional oxygen and nutrients from the perilimbal vascular system. The direct exposure of the tear film to air is crucial for maintaining the oxygen supply and corneal homeostasis undisrupted. In cases of contact lens wearing, especially with reduced gas permeability, less oxygen reaches the cornea and the corneal metabolism changes from aerobic to anaerobic. The epithelial hypoxia is responsible for lactate accumulation, which in combination with hypercapnia (carbon dioxide build-up), may account for corneal stroma acidosis, increased stromal osmotic pressure and subsequent oedema. Moreover, corneal hypoxia and hypercapnia, due to contact lenses, accounts for injection of the limbal vessels, subepithelial or deep stromal neovascularization and endothelial dysfunction (attributed also to decrease in pH at endothelium) with subsequent endothelial oedema (bleb response) [12, 81, 82].

Vascular system

The cornea is an avascular tissue. However, factors deriving from the blood supply play a very important role in corneal metabolism and wound healing. The anterior ciliary artery, which is a branch of the ophthalmic artery, forms anastomoses with vessels deriving from the facial branch of the external carotid artery in the limbal region. The cornea is therefore supplied with blood components from the internal and

external carotid arteries. In certain pathological conditions, such as corneal infections, a superficial or deep stromal neovascularization may develop resulting in a loss of corneal transparency [81, 82].

Tear film and tear secretion

The tear film is speed over the ocular surface and protects the conjunctiva and the cornea from dehydration. Its components have multiple sources, which include the lacrimal gland, meibomian glands, goblet cells, and accessory lacrimal glands of the ocular surface. Regarding the cornea, the tear film serves the maintenance and protection of smooth epithelial surface. The thickness of the tear film is approximately 3 μm and its volume 6.5 µL. It consists of three layers: a superficial lipid layer (approximately 0.1 μm), an aqueous layer (approximately 7 μm) and a mucinous layer (approximately 0.02–0.05 μm).

There are several types of glands that contribute to the production of the tear film. The Meibomian glands (approximately 30 in the upper lid and 26 in the lower lid) are large sebaceous glands located at the rim of the eyelids inside the tarsal plate and are arranged vertically near the lashes. Blinking of the eyelids forces the lipids to be excreted onto the lid margin. Wax, cholesterol and fatty acid esters are the main components of the superficial lipid layer of the tear film. The accessory ciliary glands of Zeiss and Moll have a smaller contribution to the formation of the lipid layer of the tear film. The integrity of the lipid layer is crucial for the optical quality of the eye since it does not only lubricate the ocular surface but more importantly, they protect the tear film against evaporisation of the aqueous layer and they stabilize it by decreasing its surface tension.

The aqueous layer represents more than 98% of tear film volume and is secreted mainly from the primary lacrimal gland and also from the accessory lacrimal glands of Krause and Wolfring. The main lacrimal gland is located in the superior lateral corner of the orbit, immediately behind the orbital rim within the lacrimal fossa of the frontal bone. Inferiorly, it is in contact with the globe. Anteriorly, it is divided into an orbital (upper) and palpebral (lower) lobe by the lateral horn of the levator aponeurosis.

Approximately 8 to 12 excretory ducts pass downward from the main gland to open into the conjunctival sac (lateral part of the superior fornix). One or two ducts also open in the lateral part of the inferior fornix. The accessory lacrimal glands of Krause (approximately 40 in the upper fornix and 6-8 in the lower fornix) are located beneath the palpebral conjunctiva between the upper fornix and the edge of tarsus. The accessory lacrimal glands of Wolfring are near the upper border of the superior tarsus and along the lower border of the inferior tarsus. The aqueous layer contains water, electrolytes (Na+, K+ Cl–, HCO3–, Mg2+), proteins (albumin, lysozyme, lactoferrin, transferrin, ceruloplasmin), immunoglobulins (IgA, IgG, IgE, IgM), cytokines, growth factors (EGF, TGF-α, TGF-β1, TGF-β2, bFGF, HGF, VEGF, substance P), others (glucose, vitamins). The physiological functions of this layer are lubrication, antimicrobial, bacteriostasis, supply of oxygen and nutrients, mechanical clearance, regulation of cellular functions of the conjunctiva and cornea, enabling epithelial maintenance and wound healing. The main lacrimal gland has an efferent, parasympathetic innervation and functions primarily during reflex tear secretion, whereas the accessory lacrimal glands demonstrate lack of parasympathetic innervation and a non-reflex basal tear secretion. Afferent stimuli causing discharge of the brain stem lacrimal secretory neurons arise from peripheral sensory nerve endings, usually from the trigeminal nerve, but occasionally from the retina. There are two neural pathways by which impulses from the lacrimal nucleus eventually reach the lacrimal gland to induce tear secretion. The parasympathetic pathway is primarily responsible for the gross production of reflex and continuous tears. The role of the sympathetic system remains controversial.

The mucinous layer is produced largely by goblet cells in the conjunctival epithelium along with conjunctival and corneal epithelial cells. Its main components are sulfomucin, cyalomucin, MUC1, MUC4 and MUC5AC. It serves the stabilisation of the aqueous layer of the tear film.

There are four different types of lacrimation: (1) continuous tearing, produced constantly for protection and maintenance of a healthy corneal epithelium and a perfectly smooth and transparent corneal refractive surface; (2) reflex tearing, stimulated by exposure of the free nerve endings in the eye, nose, and face to light,

cold, wind, foreign bodies, or irritating gases and liquids; (3) induced tearing, which often develops as an allergically or chemically mediated response to local irritants or by direct non-synaptic parasympathomimetic action of some drugs on the cAMP-dependent signal transduction pathways in the secretory cells of the lacrimal glands; and (4) psychogenic tearing or tears of emotion. Young infants cry without shedding tears during the first days of life, and infants born prematurely may not shed tears for weeks. This delayed capacity for psychogenic weeping suggests that the connections within the central nervous system that indirectly innervate the lacrimal system are not fully developed in most newborns [8, 18, 42, 80-82].

1.1 Basic Corneal Principles: Histology and Embryology

Corneal histology

The cornea consists of the three different cellular layers and two interfaces: the epithelium, the Bowman's layer (BL), the stroma, the Descemet's membrane (DM), and the endothelium (**Fig. 1**) [81, 82].

Epithelium

The corneal epithelium is stratified, squamous and non-keratinized. It is approximately 50 μm thick at its centre (5-6 cell layers of three different types of epithelial cells). The epithelial thickness is not evenly distributed across the cornea. It is significantly thicker inferiorly than superiorly and significantly thicker nasally than temporally with a larger inferosuperior difference than nasotemporal difference. Its dense structure provides a barrier to the passage of external agents into its deeper layers, due to the presence of junctional complexes between adjacent epithelial cells. The corneal and conjunctival epithelia are continuous and together form the ocular surface. The conjunctival epithelium is also composed of non-keratinized, stratified, squamous epithelial cells; nevertheless, its characteristics differ from those of corneal epithelium [35, 81, 82, 98]. The corneal epithelium comprises:

1. *A monolayer of basal columnar cells*. Adjacent basal cells are joined and held together by desmosomes. Hemidesmosomes (zonula adherens) anchor each basal cell to the underlying basement membrane. The basal cells demonstrate mitotic activity and their daughter cells differentiate into wing cells and subsequently into superficial cells, which emerge at the corneal surface. The differentiation process lasts approximately 7 days (complete turnover), after which the superficial cells are shed into the tear film. The basement membrane is 40–60 nm thick, is composed of a pale layer (the lamina lucida) immediately posterior to the cell membrane of the basal epithelial cells and an electron-dense layer (the lamina densa). It consists primarily of collagen type IV and laminin. The basement membrane has a critical role in corneal epithelium homeostasis by modulating the levels of growth factors and cytokines as well as regulating cell polarity, adhesion and migration via its effects on the cytoskeleton.
2. *Two to three rows of wing cells*. They are joined and held together by desmosomes and gap junctions.
3. *Two layers of squamous surface cells.* They are joined and held together by desmosomes and tight junctional complexes (zonula occludens).
4. *The superficial cells*. They have numerous microvilli and microplicae. These surface projections facilitate the attachment of mucin and the tear film and have a lifespan of a few days. Afterwards, they are shed into the tear film.
5. *The limbal epithelial stem cells (LESCs)*. A special category of corneal epithelial cells is the LESCs, which reside in the basal layer of peripheral corneal epithelium in the limbal zone (palisades of Vogt). They are responsible for the maintenance of the corneal epithelium and its reconstruction in case of trauma or disease. The LESCs have a high proliferative capacity. According to the X, Y, Z hypothesis of corneal maintenance, by division of each LESC a daughter transient amplifying cell (TAC) is generated. The TACs migrate centripetally through the basal epithelium while the original stem cell remains in the basal epithelium at limbus. TACs undergo a limited number of rapid divisions in the basal epithelial layer and move anteriorly as they differentiate into post-mitotic cells that form the wing-cell layer. The wing cells then become terminally differentiated cells that form the flattened superficial squamous layer and they are eventually shed from the corneal surface into the tear film. A

summary of the X, Y, Z hypothesis of corneal maintenance would be that X (proliferation and anterior migration) and Y (centripetal migration) must equal Z (desquamation of superficial cells) for corneal maintenance. However, according to several recent experimental studies, it has been suggested that oligopotent stem cells capable of corneal maintenance also exist outside of the limbus, serving as a secondary stem cell reservoir on the corneal surface. The corneal epithelium is renewed every 7-10 days. The LESCs also serve as a junctional barrier, preventing conjunctival tissue from growing onto the cornea [35, 81, 82, 144].

Bowman's layer

The BL is a tough, acellular, membrane-like layer, limited anteriorly by the basement membrane of the corneal epithelium and posteriorly by the corneal stroma. It is approximately 12 μm thick and consists of collagen fibres (mainly type V) randomly oriented within the extracellular matrix (proteoglycans). These collagen fibres in BL are synthesized and secreted by keratocytes of the corneal stroma. That is the reason why they appear continuous with collagen fibrils of the stroma. The BL does not regenerate after trauma. Although its physiological role remains unclear, it seems to have a protective role over corneal stroma and a major contribution in maintaining the biomechanical stability of the cornea against the forces applied by intraocular pressure [35, 81, 82].

Stroma

The stroma is the thickest corneal layer (approximately 90% of corneal thickness). The biomechanical stability and transparency of the cornea are largely attributable to the anatomic and biochemical properties of the stroma. It is mainly composed of regularly orientated layers of collagen fibrils (type I > type III, type V) within extracellular matrix of proteoglycans and glycoproteins. Collagen constitutes more than 70% of the dry weight of the cornea. Pro-collagen molecules are secreted into the extracellular space by keratocytes, after which the pro-peptides at both ends are

cleaved to yield the mature collagen molecules. The collagen molecules self-assemble and form fibrils with a diameter of 10–300 nm. These fibrils further assemble into collagen fibres. The arrangement and continuous, slow turnover (production and degradation) of its collagen fibres are essential for corneal transparency. The stromal collagen fibres arrangement is actually so significant that the sclera, cornea's neighbouring tissue, which consists also mostly of collagen fibres and other matrix macromolecules, lacks transparency due to the non-uniformity in the arrangement of these fibres. Collagen fibrils of the corneal stroma are organized into bundles called *lamellae*. The number of these lamellae varies across the cornea (300 centrally to 500 at limbus). The anterior lamellae of the stroma are randomly oriented, with frequent branching and interweaving with deeper lamellae and many of them permeate BL collagen. The posterior lamellae are better organised, running from limbus to limbus along the superior-inferior or nasal-temporal meridians parallel to the corneal surface. Collagen fibres of the corneal stroma and sclera interweave in a circumferential manner, accounting for the increased thickness at limbus. The keratocytes are the main cells of the corneal stroma and exhibit a slow turnover (every 2 to 3 years). They are dispersed among the stromal lamellae. The corneal keratocytes are normally quiescent but may activate, enter cell cycle and differentiate. In response to injury, keratocytes differentiate to myofibroblasts. Myofibroblasts produce extracellular matrix, collagen-degrading enzymes, matrix metalloproteinases and cytokines for stromal tissue repair. Their ability to contract is crucial for wound contraction and closure. However, excessive myofibroblast transformation would result in stromal fibrosis and scar formation. Other cells found in corneal stroma are dendritic cells, leukocytes and macrophages [1, 11, 22, 35, 81, 82, 137].

Descemet's membrane

The DM is also an acellular membrane which consists of collagen fibrils (types IV and VIII), laminin and fibronectin. It is the basement membrane of the corneal endothelium which increases in thickness from birth (3 μm) to adulthood (8–10 μm). It is stratified into a thin (0.3 μm) non-banded layer adjacent to the stroma, an anterior

banded zone (2–4 μm), and a posterior amorphous, non-banded zone (>4 μm). The anterior banded zone is deposited in utero and the posterior non-banded zone is laid down throughout life by the endothelium. Collagen fibrils of the stroma are not continuous with those in DM. The DM is tightly adherent to the posterior stromal surface. DM rupture due to physical stress, such as compression birth injury or forces applied by intraocular pressure on an ectatic cornea, results in the penetration of aqueous humour into corneal stroma and consequent stromal oedema. DM does not regenerate. Fuchs' dystrophy is associated with an atypical striated pattern of collagen deposition in DM. Schwalbe's line at the posterior cornea represents the termination of DM (anterior edge of the trabecular zone; limit between posterior limbal zone and the cornea). Dua's layer is a recently discovered corneal layer in the deep stroma anteriorly of DM. Dua's layer is 6 to 15 μm thick, acellular and consists of five to eight lamellae of type I collagen fibres, arranged in transverse, longitudinal and oblique directions [23, 81, 82].

Endothelium

The endothelium consists of a monolayer of hexagonal, squamous cells that cover the posterior surface of Descemet's membrane. Young adults have an endothelial cell density of about 3500 cells/mm^2. The number of cells decreases at about 0.6% per year and since the endothelium cannot regenerate, neighbouring cells enlarge to fill the space of the cells that die and fall into the anterior chamber. An increase in the variability of cell area is termed *polymegathism*. Hexagonality is another morphometric parameter of the state of the endothelium. In normal healthy corneas, about 70–80% of endothelial cells are hexagonal. However, endothelial damage or loss can result in deviation from hexagonality, a state which is referred to as *pleomorphism*. The endothelium's vital role is to provide a barrier to aqueous humour and maintain corneal deturgescence (state of relative dehydration). A cell density of approximately 500 cells/mm^2 is considered critical and the cornea could develop oedema with subsequent reduction of corneal transparency. Endothelial cells are metabolically active and contain a large nucleus and abundant cytoplasmic organelles, including mitochondria,

endoplasmic reticulum, free ribosomes, and Golgi apparatus. They interdigitate and contain various junctional complexes, including zonula occludens, macula occludens, and macula adherens. In addition, gap junctions allow the transfer of small molecules and electrolytes between the endothelial cells. The interconnected endothelial cell layer provides a leaky barrier to aqueous humour. The endothelial cells contain ion transport systems that counteract the imbibition of water into the stroma. An osmotic gradient of Na+ is present between the aqueous humour (143 mEq/L) and the stroma (134 mEq/L). This gradient results in the flow of Na+ from the aqueous humour to the stroma and in a flux of K+ in the opposite direction. The Na+- and K+-dependent ATPase and the Na+/H+ exchanger are expressed in the basolateral membrane of corneal endothelial cells. Carbon dioxide also diffuses into the cytoplasm of these cells and together with water it generates bicarbonate ions (HCO3−) in a reaction catalysed by carbonic anhydrase. The HCO3− then diffuses or is transported into the aqueous humour. Coupled with this movement of HCO3− is a flux of water across endothelial cells into the aqueous humour. Given that this ion transport system is partially dependent on cellular energy, cooling of the cornea results in its thickening and in it becoming opaque. The return of the cornea to normal body temperature, however, results in restoration of its normal thickness and clarity in a phenomenon known as *temperature reversal* [81, 82].

Corneal Embryology

Epithelial cells of the cornea are derived from the epidermal ectoderm, whereas keratocytes, scleral fibroblasts, and endothelial cells are of neural crest (neuroectodermal) origin. The surface ectoderm above the neuronal optic cup invaginates to form the crystalline lens. After the lens vesicle has separated from the surface ectoderm, the epithelium on the immature lens differentiates into the corneal epithelium. Neural crest–derived mesenchymal cells migrate in the space between the lens and primitive corneal epithelium and develop into the corneal stroma, endothelium, iris, and trabecular meshwork. Many anomalies of the anterior eye segment result from impaired differentiation of these neural crest-derived tissues [81, 82].

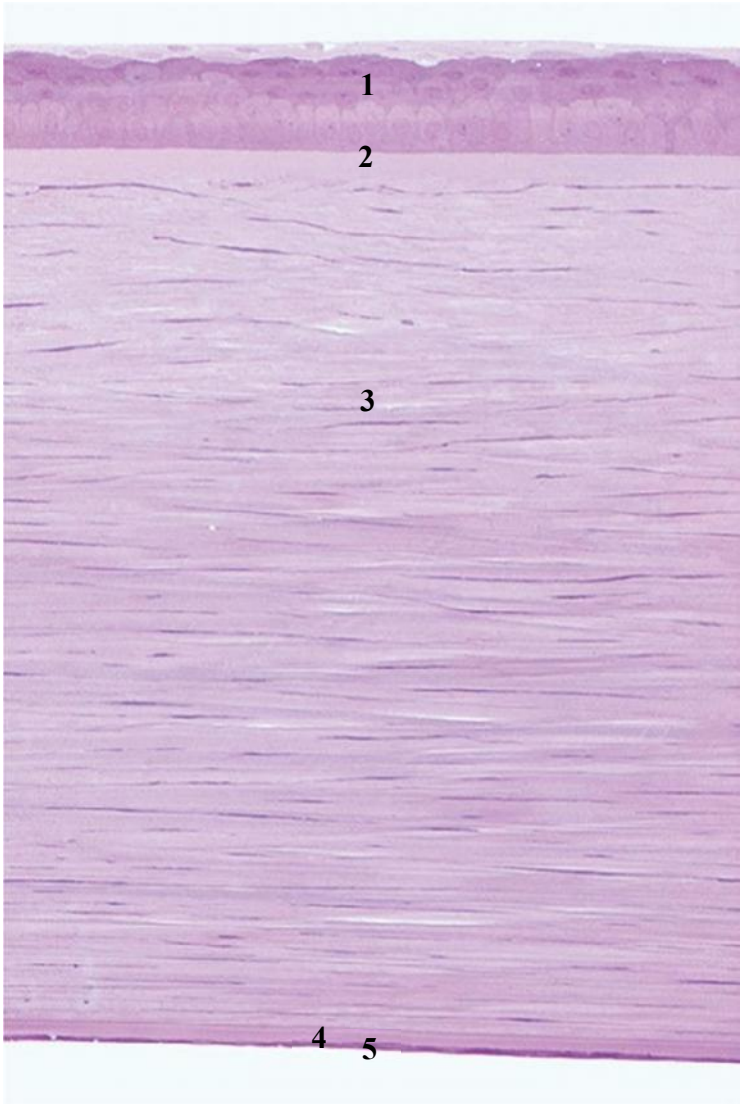

Fig. 1 Histopathological paraffin section of the human cornea, H&E stain. (1) Epithelium (2) Bowman's layer (3) Stroma (4) Descemet's membrane (5) Endothelium. Source [82]

1.2 Properties of the Cornea

Optical properties

The anterior corneal surface is convex and aspheric. Its transversely oval shape is as a result of scleralization superiorly and inferiorly. The curvature of the corneal surface is not constant, being greatest at the centre and smallest at the periphery. The radius of curvature is between 7.5 and 8.0 mm at the 3 mm central optical zone of the cornea, where the surface is almost spherical. The refractive power of the cornea is 40 to 44 dioptres (D), constituting about two-thirds of the total refractive power of the eye (60 to 65 D). Its optical properties are determined by its transparency, surface smoothness, contour, and the refractive index of the tissue. Corneal transparency is associated with the stromal collagen fibres arrangement, the small numbers of cells in stroma, the lack of vascularization, the epithelium barrier and the regulation of corneal hydration from the endothelium. In fibrosis or oedema, the distance between collagen fibrils in the corneal stroma becomes heterogeneous and the incident light rays are scattered randomly. As a result, the cornea becomes less transparent. Given that the spherocylindrical surface of the cornea has both minor and major axes, changes in corneal contour caused either by pathological conditions such as scarring, thinning, or keratoconus or by refractive surgery render the surface regularly or irregularly astigmatic. The total refractive index of the cornea is determined by the sum of refraction at the anterior and posterior interfaces as well as by the transmission properties of the tissue. The refractive indices of air, tear fluid, corneal tissue, and aqueous humour are 1.000, 1.336, 1.376, and 1.336, respectively. The refractive power of a curved surface is determined by the refractive index and the radius of curvature. The refractive power at the central cornea is about +43 D, being the sum of that at the air–tear fluid (+44 D), tear fluid–cornea (+5 D), and cornea–aqueous humour (−6 D) interfaces. Most keratometry and topography measurements assume a standard refractive index of 1.3375 [35, 81, 82].

Protective Properties

The orbit, the eyelids, the tear film, the sclera and the cornea are the mechanisms of protection of the eye against mechanical, chemical and biological insult as well as against electromagnetic radiation. The corneoscleral shell provides tensile strength to

the globe. The cornea is a barrier against microbes and prevents them from entering inside the eye. The epithelium, with the tight junctions among its cells, acts as a shield against infectious agents, fluids and solutes. The basement membrane and BL prevent infections from spreading to the stroma. In addition, the DM is resistant to proteolysis in severe corneal infections and has, therefore, a major contribution to maintaining the globe integrity in such situations. Moreover, the dense corneal innervation allows rapid blink and withdrawal reflexes. Finally, the corneal tissue absorbs nonvisible radiation (such as ultraviolet and infrared radiation), protecting, therefore, the inner structures of the eye [92, 120].

1.3 Emmetropia and Ametropia

Emmetropia

Emmetropia originates from the Ancient Greek word *εμμετρωπία* (emetropía; from *ἔμμετρος* [émmetros, "in measure"], i.e. *ἐν* - [en, "in"] + *μέτρον* [metron, "measure"], + *ὀπός* [opós, genitive of *ὄψ* (ōps) meaning "eye"]) and is the state of refraction in which the parallel rays of light, coming from a point at an infinite distance from the eye, focus on the retina, without accommodative effort. The emmetropic state is compatible with a range of refractive powers if the axial length of the eye is appropriate to its dioptric power [25, 26, 44, 107].

Ametropia

Ametropia originates from the Ancient Greek word *αμετρωπία* (ametropía; from *ἄμετρος* [ámetros, "disproportionate"], i.e. *α*- [negative prefix] + *μέτρον* [metron, "measure"], + *ὀπός* [opós, genitive of *ὄψ* (ōps) meaning "eye"]) and is a state of refraction in which the parallel rays of light coming from infinity (with accommodation at rest), are focused either in front of or behind the retina, in one or both the meridians. The ametropia includes myopia, hypermetropia and astigmatism [25, 26, 44, 107].

Myopia

Myopia or short-sightedness originates from the Ancient Greek word *μυωπία* (muōpía, "shortsightedness", from *μύω* [múō, "to shut eyes"] + *ὀπός* [opós, genitive of *ὄψ* (ops) meaning "eye"]). It is a condition in which parallel rays of light coming from infinity are focused in front of the retina when accommodation is at rest. Myopia is most commonly associated with increased axial length of the eye and is called axial myopia. The refractive myopia is associated with increased dioptric power of the eye and is subclassified into curvature myopia, due to increase of the curvature of one or more of the refractive surfaces of the eye (e.g. in keratoconus, lenticonus), and index myopia, due increase in the refractive index of crystalline lens associated with nuclear sclerosis. Index myopia is commonly observed in cases of uncontrolled diabetes (acute myopic shifts due to lenticular changes associated with hyperglycemia). Another type of refractive myopia is the anterior chamber myopia, in which a decrease in anterior chamber depth increases the refractive power of the eye [25, 26, 44, 107].

Hypermetropia

Hypermetropia originates from the Ancient Greek word *ὑπερμετρωπία* (ypermetrōpía, "farsightedness", from *ὑπέρμετρος* [hupérmetros, "excessive"], i.e. *ὑπέρ-* [hupér, prefix "hyper" meaning "over"] + *μέτρον* [metron, "measure"], + *ὀπός* [opós, genitive of *ὄψ* (ops) meaning "eye"]). It is the refractive state of the eye in which the parallel rays of light coming from infinity are focused behind the retina (i.e. the posterior focal point is behind the retina) with accommodation being at rest. Common causes of hypermetropia are the short axial length of the eye (axial hypermetropia), as well as the decreased converging power of cornea or lens (flattened cornea; increased thickness of lens). Hyperopic shifts may be observed during treatment of hyperglycaemia in diabetes [25, 26, 44, 107].

Astigmatism

Astigmatism originates from the Ancient Greek word *αστιγματισμός* (astigmatismós, from *α-* [negative prefix] + *στίγμα* [stígma, "mark, point"]). It is a refractive anomaly in which the refractive power of the astigmatic eye varies in different meridians. Consequently, the rays of light entering in the eye cannot converge to a single point on the retina but form focal lines. The image is formed as a Sturm's conoid. It is broadly classified into regular astigmatism, in which the principal meridians are at 90° to each other, and irregular astigmatism, in which the principal meridians are not at 90° to each other. Irregular astigmatism cannot be corrected with spectacles. Corneal astigmatism is the result of abnormalities of the corneal curvature and is the most common cause of astigmatism. Lenticular astigmatism is the result of curvature abnormalities of the lens (e.g. lenticonus). The regular astigmatism is classified into the following types:

1. *With-the-rule astigmatism*. If the corneal meridian that has the least refractive power is horizontal (180° ± 20° degrees), that is, between 160 and 20 degrees, this is described as with-the-rule astigmatism. Thus, correction of this astigmatism will require the concave (minus) cylinders at 180° ± 20° or convex (plus) cylindrical lens at 90° ± 20°. It is called 'with-the-rule' astigmatism because similar astigmatic condition exists normally (the vertical meridian is normally rendered 0.25 D more convex than the horizontal meridian by the pressure of eyelids).
2. *Against-the-rule astigmatism.* If the corneal meridian that has the least refractive power is vertical (90° ± 20° degrees), that is, between 70 and 110 degrees, this is described as against-the-rule astigmatism. Therefore, correction of this astigmatism will require the prescription of convex (plus) cylindrical lens at 180° ± 20° or concave (minus) cylindrical lens at 90° ± 20° axis.
3. *Oblique astigmatism.* If the corneal meridian that has the least refractive power lies either between 20 and 70 degrees or between 110 and 160 degrees, this is described as oblique astigmatism. Oblique astigmatism is often found to be symmetrical (e.g., cylindrical lens required at 30° in both eyes) or complementary (e.g. cylindrical lens required at 30° in one eye and at 150° in the other eye) [25, 26, 44, 107].

1.4 Corneal Topography

1.4.1 Curvature-Based Instruments

The anterior corneal surface is smooth, with its irregularities being neutralized by the tear film. In this case, the anterior surface acts as an almost transparent convex mirror by reflecting part of the incident light. There are many non-contact instruments, which assess the anterior surface by measuring the reflected light by using light target (in different shapes) and a microscope or other optical systems. The instruments are either quantitative or qualitative, and either reflection-based or projection-based [119].

Keratometer

A keratometer is a quantitative reflection-based instrument. It measures the corneal radius in the central 3 mm zone by measuring the size of the reflected image, and converting the image size into corneal radius using the following mathematical relationship:

$$\mathbf{r = 2aY / y}$$

(r: Anterior corneal radius; a: Distance from the mire to cornea [75 mm in keratometer]; Y: Image size y: Mire size [64 mm in keratometer]). The keratometer can convert from corneal radius r (measured in meters) into refracting power (in D) using the relationship:

$$\mathbf{Refractive\ Power = 337.5 / r}$$

Measurements of the corneal reflex may be affected by eye movement, decentration or tear film deficiency. Videotopographers, on the other hand, can freeze the reflected corneal image, and perform the measurements once the image is captured on the video or computer screen, allowing greater precision [119].

Keratoscopy or Photokeratoscopy

While the keratometer analyses approximately 6% of the anterior corneal surface, the keratoscope measures 70% of the total anterior corneal area (limited by the optical system of the machine itself). A photokeratoscope is a qualitative reflection-based instrument and the projected light may be a simple flashlight or a Placido disk target. The Placido disc is a series of concentric rings (10 or 12 rings) or a cone with illuminated rings lining the internal surface of the instrument. According to changes in the shape of the reflected rings and the spaces in between, we may appreciate the shape of the cornea (i.e. small, narrow and closely spaced rings suggest steep regions with a small radius of curvature). The use of photokeratoscope has many disadvantages. Specifically, it requires assumptions about the corneal shape, misses data from the central cornea (not all instruments), acquires data from limited points on the corneal surface, measures corneal curvature but not height, measures only the anterior corneal surface, is affected by defocus and misalignment and is severely affected by tear film disturbances. Nowadays, the use of the photokeratoscope is being abandoned and replaced by computerized topographers, which allow both qualitative and quantitative measurements [119].

Computerized Videokeratoscopy

This is one of the modern topographers. The modern topographers are based upon projecting (not reflecting) images. Basically, a projection-based topographer consists of a Placido disk or cone (small or large), which projects a mire of concentric light rings, a video camera that captures the reflected rings from the tear film layer and a software to analyse the data. The computer evaluates the distance between the concentric rings (dark and light areas) in a variable number of points, with a shorter distance corresponding to higher corneal power, and vice versa. After analysing the data, they are plotted by the computer as a colour map. The Placido cone may be large or small according to the manufacturer. A larger the cone has more the rings and may evaluate a wider area. The mires of most systems exclude the very central cornea and paralimbal corneal region. The reproducibility and validity of videokeratographic measurements are mainly dependent on the accuracy of manual adjustment in the focal plane [119].

1.4.2 Elevation-Based Topographers

Placido-based (or curvature-based) systems rely on the data from the anterior corneal surface and are reflection-based or projection-based. Additionally, without the information about the posterior surface, they cannot provide a complete pachymetric evaluation of the cornea. Although ultrasonic pachymetry can give us central and few paracentral measurements, a full pachymetric map is mandatory in modern corneal refractive surgeries. Moreover, the posterior surface of the cornea is a more sensitive indicator of corneal ectasia and can often be abnormal in spite of a normal anterior corneal surface. Furthermore, in the curvature-based systems, the elevation map of the anterior surface is derived from the curvature map, while it is directly calculated in the elevation-based systems [119].

Description of Pentacam

Pentacam™ (Oculus Optikgeräte GmbH, Wetzlar, Germany) utilizes a rotating Scheimpflug camera. During the rotation, the camera generates Scheimpflug images in three dimensions. Pentacam illuminates the cornea perpendicularly and analyses the corneal cross-section from an angle of ± 45°. It takes a maximum of 2 seconds to generate a complete image of the anterior eye segment. Any eye movement is detected by a second camera and corrected for in the process to some extent. The Pentacam calculates a 3-dimensional model of the anterior eye segment from as many as 25000 true elevation points (Pentacam HR: 138000 points). The topography and pachymetry of the entire anterior and posterior surfaces of the cornea from limbus to limbus are calculated and depicted [79, 119].

1.4.3 Corneal Maps generated by Pentacam

Corneal Thickness Map

The Pentacam software evaluates the thickness of the cornea at all points based on the elevation maps. The difference between the front and back surface elevations indicates corneal thickness. Pentacam measures the distance between the anterior and posterior corneas normal to the anterior surface. Corneal thickness maps provide useful information for diagnosing ectatic diseases of the cornea, such as keratoconus, pellucid marginal degeneration and iatrogenic ectasia, and are crucial when designing a corneal refractive treatment or evaluating the outcome of corneal transplantations and corneal refractive surgery. The software provides information about the central thickness at the corneal apex (CA), the corneal thickness at the pupil centre, the minimum corneal thickness as well as the thickness at any other point within the map display. Different values are presented with different colours, resulting in a unique and easily interpreted pattern. The software also provides information on the exact coordinates of each measured point, with the CA representing the origin point (zero point). The software can also generate differential corneal thickness maps from two consecutive measurements, presenting, therefore, changes of corneal thickness. The differential corneal thickness maps are commonly used for assessing the spatial distribution of the extracted lenticule or photoablated tissue in the corneal stroma after corneal refractive surgery [116, 133].

Other clinical interpretations of the corneal thickness maps involve the shape of the map (e.g. conic shape in keratoconus or bell shape in PMD), the superior-inferior ratio (S-I) on the central 5 mm circle (symmetric superior and inferior values should be compared; differences S-I > 30 μm may indicate ectasia), the difference in thickness of the thinnest location between both eyes (> 30 μm is considered abnormal), and the difference in thickness between the thinnest location and the apex (> 10 μm is suspicious for corneal ectasia). One limitation of corneal thickness map is that the measurements are affected by corneal opacities. The effect of a corneal opacity presents itself on corneal thickness map as artefacts, which might appear as focal thickening or more commonly focal thinning [116].

Regarding corneal refractive surgery, the corneal thickness is an important factor that determines the amount of the photoablated or extracted tissue. The corneal thickness, the degree of myopia, and the residual stromal bed are inter-related. Low

corneal thickness is a risk factor for iatrogenic ectasia. Since keratoconic corneas are thinner than normal corneas, thin corneas may be an indicator of early keratoconus, and thinner corneas are at higher risk for low residual stromal bed thickness due to variability in microkeratome function. However, preoperative corneal thickness alone appears to be only a weak indicator for increased risk of ectasia, with laser-assisted in situ keratomileusis (LASIK) being successfully performed in corneas less than 500 μm without incident. Therefore, there does not appear to be a clear cut-off value below which LASIK cannot be safely performed if all other factors are normal. Biomechanical studies have reinforced the importance of residual stromal bed (RSB) thickness after corneal refractive surgery. Both stress-strain analysis and cohesive tensile strength analysis indicate that corneal strength is significantly greater in the anterior 40% of the corneal stroma than in the posterior 60%. Furthermore, the corneal flap contributes minimally to the tensile strength of the cornea after LASIK. Thus, LASIK reduces corneal structural integrity both by reducing overall available load-bearing tissue and by shifting the load bearing responsibility to the structurally weaker posterior corneal stroma. It is clear, however, that RSB of 250 μm does not absolutely discriminate between eyes that will develop ectasia and those that will not. Rather, RSB seems to be a continuous variable, with the risk of ectasia increasing with decreasing RSB [96, 116].

A more important metric for evaluation of ectasia risk is the percentage of tissue altered (PTA). This metric provides information about the alterable biomechanical properties, through the amount of tissue altered by corneal refractive surgery and the remaining load-bearing tissue. The PTA can be described for LASIK as:

$$\mathbf{PTA = (FT + AD) / CCT}$$

(FT: flap thickness; AD: ablation depth; CCT: central corneal thickness). A high value of PTA, especially >40%, is a relevant factor in the development of post-LASIK ectasia in eyes with normal preoperative Placido disk-based topography, and therefore, PTA should be taken into account as a screening parameter for refractive surgery candidates. The small incision lenticule extraction (SMILE) technique, however, utilizes different principles for reshaping the cornea in order to modify its refractive power. Taking into consideration the intact anterior stroma lamellae, the PTA as described for LASIK,

does not accurately represent the percentage of altered tissue after SMILE (**Fig. 2**). Therefore a modified PTA (mPTA) formula has been suggested for SMILE. The mPTA can be described as:

$$\mathbf{mPTA = (S \times CT + LT) / CCT}$$

(S: small-incision length to total SMILE cap circumference; CT: cap thickness; LT: lenticule thickness; CCT: central corneal thickness) [73, 108].

Curvature Maps

The cornea is aspheric and the radius of curvature is not equal at all points. In order to measure the refractive power of the cornea, it is necessary to measure the radius of curvature at any given point. There are two methods for measurement of corneal curvature: 1) the sagittal (axial) method, and 2) the tangential (local) method.

Sagittal (axial) map

In order to measure the refractive power at point "a", a tangent is drawn on the surface of the cornea at that point. The "normal" of that tangent intersects with the measurements reference axis at point "b". The segment "ab" represents the curvature radius of the cornea at point "a". The refractive power of the cornea at that point is calculated by the following equation:

$$\mathbf{Corneal\ Power = (n1–n2) / r}$$

(n1: refractive index of the spherical refractive surface, supposed to be the surface of the cornea; n2: refractive index of air, in front of the cornea; r: curvature radius of the refractive spherical surface, supposed to be the surface of the cornea). The software displays this power as a coloured map with a colour scale. This is applied on the front and back surfaces of the cornea. Values of the back corneal surface power are displayed as negative values because the posterior surface functions as a concave surface [117].

Tangential (local) Map

In the tangential map, circles are formed tangentially to the examined corneal surface at the points to be measured. The radius of the best fit tangential circle is considered as the curvature radius, on which the equation can be applied. Radii of circles differ according to surface changes. Geometrically, the specifications of the tangent circles are more accurate than those of the tangent lines. Therefore, the tangential map is more susceptible to local curvature changes and can highlight minor irregularities of the cornea. Moreover, each point on the tangential map is calculated independently, i.e. there is no reference axis. Therefore, the map data are, to some extent, less affected by misalignment during image acquisition. In addition, the tangential map is better for evaluating corneal periphery. In general, curvature maps are affected by tear film disturbances and use of contact lenses [117].

Elevation Map

The Pentacam software suggests a reference body for each corneal surface. The reference body of the front surface may differ from that of the back surface, although both surfaces are of the same cornea. The software adjusts the reference surface with the measured surface. All points above the reference surface are considered elevations and are displayed with positive values, while the measured points below the reference surface are considered as depressions and are displayed as negative values. The coincidence points between the reference surface and the measured surface are displayed as zeros. There are 3 types of reference bodies, which could be selected to generate the elevation map:

1. *The Ellipsoid Body*. It is an aspherical body which is rotationally symmetric according to two axes, major and minor. It has a coronal rounded cross-section and helps in highlighting the real shape of the cornea.
2. *The Toric Ellipsoid Body*. It is an aspherical shape which is rotationally symmetric according to two axes, major and minor. But it has a coronal elliptical cross-section, i.e. there are two perpendicular axes, one is steeper than the other. Its advantage consists in the very good approach to the real course of, e.g. astigmatic corneal surface.

3. *The Spherical Body.* It is better than the previous bodies in highlighting corneal irregularities since the normal cornea has a toric ellipsoid shape. It is well known that to recognize something, it should be matched with other different things. Therefore, if we want to show the details of an abnormal cornea, we should relate it to a spherical reference body.

The reference body can be adjusted with the examined surface of the cornea in various locations. Accordingly, details of the central part might appear (or disappear). If the reference body is adjusted in contact with the apex of the cornea, it is called "no float mode". On the other hand, when the reference body is represented to be optimized with respect to the cornea, it is called "float mode", i.e. the distance between the two bodies (corneal surface and reference body) should be equal in sum and minimum. The float mode is most commonly used as a standard to compare examinations carried out by various topographic systems. Unfortunately, very early stages of keratoconus are difficult to recognize on the float shape due to distance optimized adjustment. That is because when a reference body is adjusted in contact with the CA, any bulge near the apex will be relatively visible, and vice versa, any small bulge might be lost among larger details when the reference body is adjusted away from the apex [118].

1.5 Refractive Surgery

Refractive surgery aims at changing the refractive status of the eye. Refractive surgery can be broadly classified into corneal refractive surgery and lenticular surgery. The lenticular surgery involves implantation of phakic intraocular lenses (IOLs) (e.g. implantable collamer lenses, anterior chamber angle-supported phakic IOLs and anterior chamber iris-fixated phakic IOLs) as well as clear lens extraction with implantation of monofocal, multifocal or extended depth of focus IOLs. On the other hand, corneal refractive surgery attempts to reshape the cornea in order to modify its refractive power. Early methods of reshaping the cornea involved radial keratotomy, with radial incisions that resulted in peripheral elevation central corneal flattening (increased effect with deeper and more central incisions).

The use of *lasers* (light amplification by stimulated emission of radiation) in ophthalmology enabled more precise corneal refractive techniques with higher repeatability and stability of the refractive outcome. In 1988 Munnerlyn et al. introduced the photorefractive keratectomy (PRK) as a technique for refractive surgery with the use of an excimer laser. Two years later, in 1990 Professor Ioannis Pallikaris introduced LASIK with the use of a modified microkeratome for the creation of central corneal flaps and an ArF excimer laser for circular ablation. The advent of femtosecond lasers enabled unparalleled precision in flap creation, with the femtosecond laser–assisted LASIK (FS-LASIK) demonstrating excellent accuracy, efficacy and repeatability. Moreover, femtosecond laser technology enabled the intrastromal, all-in-one femtosecond laser procedures. In 2008 Professors Walter Sekundo and Marcus Blum introduced and reported the first outcomes of the femtosecond lenticule extraction (FLEx) for the correction of myopia. The true revolution, however, came a few years later when the same group introduced the SMILE technique. Ever since then, SMILE has been gaining increasing acceptance among refractive surgeons due to its advantages over FS-LASIK regarding corneal biomechanical stability, postoperative dry eye, surgically induced corneal higher order aberrations (HOA), and contrast sensitivity (**Fig. 2**) [32, 36, 45, 47, 69, 77, 87, 88, 99, 110-112, 122, 136]

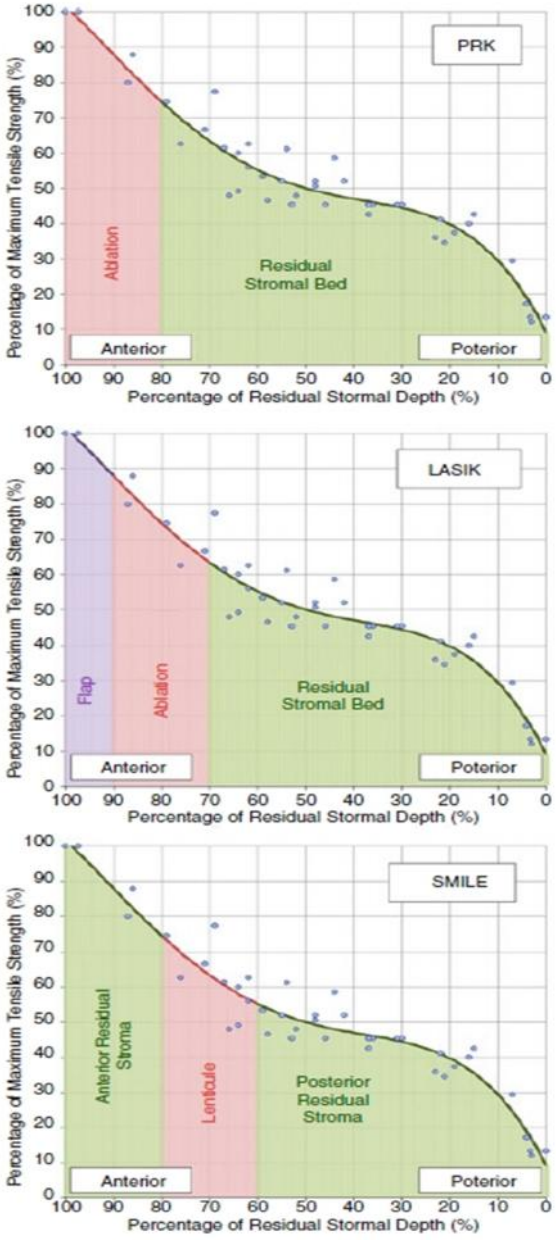

Fig. 2 Scatter plots of the percentage of maximum cohesive tensile strength against the percentage of residual stromal depth. The fourth-order polynomial regression equation was integrated to calculate the area under the curve for the relevant stromal depths after PRK, LASIK, and SMILE as demonstrated by the green shaded regions. The red areas represent the tissue removed (excimer laser ablation/lenticule extraction) and the purple area in LASIK represents the LASIK flap. Source [99]

1.5.1 Small Incision Lenticule Extraction

Basic Principles

SMILE is an all-femtosecond laser, intrastromal, refractive procedure [110, 112]. The 1.053 nm wavelength of light used by the femtosecond laser produces a tissue interaction, known as photodisruption. The photodisruption is induced by ultra-short laser pulses (pulse duration in the femtosecond range). During the photodisruption process, plasma (free electrons and ions), an acoustic shockwave, thermal energy, and then a cavitation bubble are created. This process of photodisruption, termed laser-induced optical breakdown, essentially vaporizes a small volume of tissue. The threshold for photodisruption is inversely related to the laser's intensity i.e. the shorter the pulse's duration, the smaller the diameter of the laser spot, the lower the energy needed for photodisruption. The femtosecond laser permits the creation of corneal cuts of different shapes, at desired depths, but the fundamental requirement for this is corneal transparency that allows the precise focus of the laser spots. The corneal surface is the reference plane for the laser. A lens with a higher numerical aperture will create a more focal laser spot in terms of its diameter and volume, which enhances the depth accuracy and overall precision of the lamellar cut. The VisuMax® system (Carl Zeiss Meditec AG, Jena, Germany) is the only available platform for SMILE. It uses a high numerical aperture lens with lower pulse energy and higher pulse frequency (500 kHz). Lower pulse energy is generally associated with fewer unwanted side effects, such as an opaque bubble layer, collateral thermal damage, corneal inflammation, and diffuse lamellar keratitis as well as transient light sensitivity [64].

The SMILE procedure involves two steps: the femtosecond laser application for the creation of the intrastromal lenticule and the manual removal of the lenticule. The VisuMax femtosecond laser has its unique curved suction contact glass that allows minimal distortion of the cornea and minimal elevation of the intraocular pressure during suction (up to 70-80 mmHg; i.e. not higher than the normal diastolic blood pressure). The suction contact glass comes in three sizes (S, M, L) based on the white-to-white diameter of the cornea. The recommendation of the company for SMILE is the

S size contact glass, which allows a lenticule diameter up to 7.8 mm (usually a diameter of 6.5mm is used) and a cap diameter of up to 7.9 mm [10, 72]. The procedure begins with the docking and suction of the globe with the use of the suction contact glass and vacuum. SMILE involves four cuts: (1) the posterior plane cut (refractive plane), (2) the lenticule edge cut, (3) the anterior plane cut, and (4) the entrance wound cut. The required instrumentation for SMILE involves an eyelid speculum, absorbent surgical spears, sterile balanced salt solution (BSS; 15 cc bottle), blunt irrigating cannula, a double-ended lenticule dissector with a Sinskey-like hook at the other end and a microforceps for lenticule extraction. Virtually every ophthalmic instrument manufacturer has its own set. After the femtosecond laser cuts are completed, the surgeon enters the peripheral incision with a Sinskey-like hook and breaks the tissue bridges with a dissector by bluntly dissecting in the plane between the lenticule and the stromal cap and that between the lenticule and the stromal bed. The anterior plane is separated first, followed by the posterior plane. The initial separation of the posterior lenticule surface may not be considered a wrong approach. Some experienced surgeons routinely perform the posterior dissection before the anterior dissection. However, for the novice SMILE surgeon, this may result in complicated lenticule extraction. After the separation of both planes, the lenticule is retrieved and removed from the pocket using the forceps. While some surgeons prefer to flush the pocket with BSS in order to remove any possible remained interface debris (cellular constituents), some others consider this step unnecessary [15, 28].

Advantages of SMILE over other corneal refractive techniques

The major advantage of SMILE is the greater postoperative tensile strength compared to FS-LASIK and PRK, especially when treating higher degrees of myopia. In SMILE the anterior stroma lamellae and the BL remain almost intact (with the exception of the lamellae and BL at the site of the peripheral incision, which, however, represents a small portion of the cap's circumference). Randleman et al. investigated the cohesive tensile strength in human donor corneas and resulted that the anterior 40% of the central corneal stroma is the strongest region of the cornea, whereas the posterior

60% of the stroma is at least 50% weaker [94]. Theoretically, therefore, tensile strength and biomechanical stability are better preserved after SMILE, compared to FS-LASIK and PRK, which involve cut or ablation of the BL and anterior stroma. This assumption has been further supported by mathematical models and clinical studies, which showed increased biomechanical properties after SMILE compared to other corneal refractive techniques [99, 136]. Moreover, in a recent ex vivo study on porcine corneas, it was shown that the cap-based SMILE technique may preserve the corneal biomechanical properties better compared to flap-based procedures such as FLEx. [122]

Another significant advantage of SMILE is that it induces less inflammatory and wound healing responses [48]. Specifically, it has been shown that after all-femtosecond laser-assisted procedures there was little or no expression of early inflammatory markers in the central stroma and moreover, their number remained stable regardless of the power of the correction. On the contrary, after FS-LASIK the expression of early inflammatory markers increased significantly when high power corrections were performed and cornea reflectivity, as examined with IVCM, showed more intense and abundant light-scattering particles as a result of the photoablation process [104]. Dong et al. showed that SMILE may stimulate less keratocyte proliferation and tissue inflammation compared to FS-LASIK. Moreover, greater keratocyte apoptosis was induced after FS-LASIK, probably due to flap lifting and greater contact of the bare stroma with cytokines induced by the epithelial trauma [21]. Another major experimental study was recently presented by Liu et al., investigating the postoperative wound healing response after hyperopic SMILE, hyperopic SMILE without lenticule extraction and hyperopic FS-LASIK. The authors concluded that hyperopic-SMILE induced less postoperative wound healing response and stromal interface reaction compared to hyperopic FS-LASIK, especially in higher refractive corrections. Furthermore, the keratocyte response was upregulated after hyperopic SMILE when compared to hyperopic SMILE without lenticule extraction, suggesting that the surgical manipulation, rather than the laser interaction, may induce cellular stress in the surrounding stromal tissue [63].

Patients after SMILE seem to be less affected by dry eye. In a recent meta-analysis, it has been shown that SMILE exhibits a lower risk of postoperative dry eye

compared to FS-LASIK. In addition, the SMILE procedure induces fewer negative impacts on the ocular surface and corneal innervation compared to FS-LASIK [45]. In SMILE, after the creation, dissection and extraction of the lenticule, stromal nerve fibres within it are resected. However, the procedure results in less damage of the subepithelial nerve plexus and therefore, better corneal sensitivity and reduced dry eye symptoms [67].

Last but not least, performing an all-femtosecond laser-assisted technique like SMILE or FLEx enables the preservation of the extracted lenticules, thus, rendering these procedures as potentially reversible. Cryopreserved or fresh stromal lenticules have been successfully used in for autologous re-implantation and allogeneic implantation in laboratory animals and human subjects in order to reverse a myopic correction, treat presbyopia, hypermetropia (primary or due to aphakia) and keratoconus. The use of stromal lenticules has also been described for therapeutic purposes with an allogeneic lenticule being transplanted under a LASIK flap in order to restore corneal volume and thickness and reduce the refractive error in a case of excessive stromal tissue removal after LASIK [31, 39, 50, 51, 65].

Complications and Challenges of SMILE

Intraoperative complications in SMILE include suction loss, minor/major tear at the incision, abrasion at the incision, incomplete lenticule dissection (e.g. due to black spots), lenticule extraction difficulties, creation of a wrong deeper dissection plane by forceful manual dissection (so-called via falsa), lenticule tear, retained lenticule or lenticule fragment, cap perforation and decentration of optic zone. Postoperative complications include mild postoperative haze, dry eye in the short-term, epithelial ingrowth, foreign bodies at the interface (e.g. fibres), interface inflammation, keratitis, monocular ghost images associated with corneal irregularities and HOA (e.g. coma and spherical aberration), and residual refractive error. Though iatrogenic ectasia after SMILE has been reported, it was mainly associated with pre-existing subclinical keratoconus [28, 38, 73].

Suction loss is a major challenge in SMILE and is associated either with wrong head positioning (e.g. contact of the nose with the gantry) or if the patient is too nervous to maintain fixation (e.g. abrupt head or eye movement). The pooling of fluid (tears, BSS, anaesthetic) in the fornices may also predispose to suction loss due to fluid ingress between the suction ports of the contact glass and the cornea. It is, therefore, recommended to remove the excess fluid using an aspirating speculum or with a sponge, without, however, drying the cornea excessively as this can hamper applanation and docking. A loose bulbar conjunctiva may prolapse toward the cornea and increase the incidence of suction loss. This also can block the laser delivery, especially the incision at 12 o'clock position. In such cases, it is recommended to use a solid blade speculum and applanate the cornea fully before putting on the suction. Many cases of suction loss are associated with patient anxiety and unsteady gaze. It is, therefore, important to converse with the patients so that they know the steps of the procedure and what expect. Finally, gas bubble migration during the lenticule formation may produce compressive forces against the contact glass and result in suction loss [33, 62 113]. In the event of a suction loss, the VisuMax automatically goes into a specific mode, based on the stage of the procedure at which the suction loss occurred. In case the suction loss occurs during the first pass of the laser (i.e. posterior surface of the lenticule), the user is not given the option to complete the procedure and is asked to convert the procedure into a FS-LASIK procedure. The user may perform the FS-LASIK in the same surgical session. It is also possible to postpone the procedure for a few minutes or days and then repeat SMILE with a reduced cap in order to avoid entering of the old incision. If the suction loss occurs at any other stage during the laser firing procedure, the laser allows the option of completing the procedure in the same surgical session after re-docking of the contact glass. In this case, the new centration should be aligned with the previous one. It is preferable to use the same contact glass so that the footprints of the contact glass match. Proper centration during re-docking is extremely important. Once re-docking is completed, depending on the stage at which suction loss occurs, the laser may repeat both passes, only the second pass or only the side cut incision [100, 113].

Difficulties in lenticule extraction pose another challenge during SMILE. An initial separation of the posterior lenticule surface may result in complicated lenticule extraction. In cases of retained lenticules, which are uniformly spread and attached to the cap as a result of initial posterior plane dissection, management would require the identification and separation of the anterior plane. This could be performed by gently dissecting a small edge of the lenticule from the cap's posterior surface using a Sinskey hook. This could be accomplished on either side of the incision rather than its centre because the uncut edge of the incision on both sides allows the Sinskey hook to be introduced more easily. Once a small pocket is created at the anterior plane, the dissector can be introduced and the lenticule can be separated and extracted in the usual manner [28, 113].

Lenticule tears present also a challenging situation. This is more common when treating low myopia because of the reduced lenticule thickness. Theoretically, the lenticule thickness may be estimated by Munnerlyn's formula:

$$t = S^2 D / 3$$

(t: thickness of the tissue ablated in μm, S: diameter of the optical zone in millimetres, D: dioptric correction), whereby the rule of thumb is: 1 D correction at the 6 mm zone corresponds to 12 μm tissue thickness. In myopia correction, this measurement presents as the central thickness of the lenticule; in hyperopia correction, it presents as the thickness of the lenticule at the edge of the optical zone. The extraction of a lenticule of reduced thickness would be very challenging. For that reason, VisuMax adds a refractive neutral, parallel tissue layer of 10-15 μm at the posterior surface of the lenticule. Although this translates to slightly higher tissue removal of the SMILE procedure compared to LASIK or PRK, it is necessary in order to minimize the risk of lenticule tear and make the dissection and extraction easier. The general recommendation for the minimal lenticular thickness is 30µm [9, 77, 100].

In the event of a lenticule tear associated with incomplete photodisruption due to black spots or massive opaque bubble layer, a prompt surgical exploration for removal of the retained tissue is necessary. Peripheral retained fragments pose no threat to visual rehabilitation and visual acuity due to their location and reduced thickness. However, central retained fragments would compromise the visual outcome, thus requiring

immediate surgical exploration for their removal, before the fragment becomes fibrotic and develops strong adherence with the interface surfaces. When the photodisruption of a small area is not optimal, the surgeon could attempt a manual delamination with the Reinstein lenticule separator or any dissector with a sharp cutting edge. However, forceful manual dissection could result in the creation of a deeper dissection plane and greater stromal tissue trauma at the interface. Moreover, forceful manipulations may cause tearing of the incision, which increases the risk of epithelial ingrowth. If the clinical findings suggest an area where no photodisruption was accomplished (i.e, corresponding to a large black spot), then the situation would be more complicated, especially if this area is large and located near the visual axis. In this case, if the lenticule is not folded or dislocated and does not induce irregular astigmatism, a re-treatment with SMILE or conversion to FS-LASIK at least 6 months later may be performed. However, if the retained lenticule induces irregular astigmatism, then a topography-guided PRK with mitomycin C should be performed for regularization of the corneal surface [28].

In the event of a cap tear, if the tear is small and outside the pupillary area, it has no adverse outcome other than a small scar. If the tear is large, the surgeon should align the anterior surface properly and place a bandage contact lens on. In cases of cap or incision tears, there is a higher risk of epithelial ingrowth. In order to avoid tears of the cup or the incision, the surgeon should fixate the globe and use a larger incision [113].

In SMILE there is a tendency to undercorrection, especially in high degrees of refractive errors. In order to avoid residual refractive errors after SMILE nomogram adjustments based on the degree of the refractive error and age should be applied [33, 37, 58, 71]. The undercorrection of astigmatism may be associated with the effect of cyclotorsion. The VisuMax does not have cyclotorsion compensation, but it is important to correct for cyclotorsion in higher cylinders. Cyclotorsion may occur for various reasons, such as (1) cyclotorsion occurring naturally from sitting to supine position, (2) positioning of head and turning the face, (3) speculum placement and patient's resistance to it as well as Bell's phenomenon, and (4) applanation and suction can induce cyclotorsion due to difference in the corneal curvature and curvature of the interface. In order to manually compensate for cyclotorsion, the 0–180° axis is marked

on the limbus extending about 2 mm on either side onto the cornea with the patient sitting upright. Following applanation and suction, the surgeon should check for the alignment of the 0–180° marks with respect to the horizontal line on the reticule through the microscope or on the VisuMax screen. Then, the suction cup should be rotated so that it is aligned with the marks before proceeding with the laser delivery. Cyclotorsion should be corrected when the cylinder of the correction is greater than 0.5 D. Also, as suggested by empirical nomograms the with-the-rule cylinder should be 10 % overcorrected. The use of an optical zone larger than 6.5 mm may result in good postoperative outcomes even in high cylindrical corrections [30, 33].

1.5.2 Femtosecond laser–assisted LASIK

Basic Principles

The term keratomileusis origins from the Greek word *κερατοσμίλευση* (keratosmílefsi, "cornea carving", from *κέρας* [kéras, "horn"] + *σμίλευση* [smílefsi, "carving"]) and was first used by Professor José Ignacio Barraquer, who suggested that the surgical addition or removal of corneal tissue could change the curvature of the air/tear film interface, where the two thirds of the refractive power of the eye is located. The myopic keratomileusis was introduced by Barraquer in 1949. The initial procedure involved creating a lamellar corneal disc approximately 300 μm in depth (lamellar keratectomy) and removing tissue from the residual stromal bed or the disc (refractive keratectomy). When the disc was replaced, the anterior corneal curvature was flattened, thus reducing the refractive power of the eye and correcting myopia. Both keratectomies were initially performed freehand with a Paufique knife. Removing stroma from the bed freehand proved to be technically difficult and very inaccurate that Barraquer temporarily abandoned the in situ technique [6, 85].

The LASIK technique was developed and introduced by Professor Ioannis Pallikaris at the University of Crete in 1988 and involved the creation of a flap with a microkeratome and subsequent ablation of the stromal bed with the use of an excimer laser [87, 88]. LASIK was considered a revolutionary procedure, which had significant

advantages over PRK such as faster visual rehabilitation, minimal postoperative pain, lack of adverse healing phenomena such as haze formation, and increased range of efficacy over PRK in high myopia, hyperopia, and astigmatism [85].

Since 2003, the use of femtosecond lasers for flap creation produced equal or better outcomes compared to microkeratomes, enabling higher precision and better reproducibility of flap thickness [84, 97, 124, 126]. The flap cut is created by the femtosecond laser with photodisruption. This is the same principle as previously described for the lenticule formation in SMILE [64]. The photodisruption is performed under suction of the globe using a suction ring, which stabilizes the eye with the application of vacuum. As mentioned before, the VisuMax femtosecond laser has its unique curved suction contact glass. It comes in three sizes (S, M, L) based on the white-to-white diameter of the cornea. For a minimum white-to-white diameter of 11.2 mm it is advised to use the S size, for a minimum of 11.7 mm the M size, and for a minimum of 12.4 mm the L size. The smallest possible suction contact glass should be selected [72]. The selection of suction ring for other platforms may be based on keratometric values, with research groups recommending a 9.5-mm suction ring for typical cases, a 9.0-mm suction ring when the keratometric value K1 is > 46 D, and a 10.0 mm suction ring when the keratometric value K1 is ≤ 41 D [46]. After creation of the flap, the suction is released and the flap is lifted. Before lifting the flap, the surgeon may apply peripheral marks for more accurate repositioning. After lifting the flap, the stromal bed is prepared (flushed with BSS and wiped with wet microsponges) for the photoablation.

The ablation is performed with the use of an argon fluoride (ArF) *excimer laser* (excited dimer). The ArF excimer laser has a wavelength of 193 nm, which imparts energy of 6.4 eV per photon. This photon energy is adequate to break covalent bonds between collagen molecules through the process of ablative decomposition. Krueger et al. compared the tissue effects of different gas dimers used in excimer lasers and found that the 193 nm ArF wavelength provided smoother results, more precise ablation, and decreased thermal damage to adjacent tissue. For these reasons, the excimer ArF laser is the laser of choice for LASIK and PRK. There are three approaches to refractive photoablative decomposition: (1) scanning slit, (2) wide area (broad-beam), and (3)

flying spot. Currently, the broad-beam excimer lasers have been abandoned mainly because of laser-induced deviations from the intended uniform corneal profiles, which increased the ablation depth and decreased the predictability of the refractive outcomes. Other major limitations were the biological interactions and wound healing responses, which are considered to be key factors that reduce the outcome predictability and may contribute to haze formation. The new generation of excimer laser platforms has reduced the amount of time and tissue ablated by delivering more laser spots per second and ablating more corneal tissue in a given time. In the 6th generation lasers, for instance, the speed (frequency) varies from 400 to 1050 Hz. On average, a 500 Hz platform will reduce the ablation time needed per D in a 6.5 mm optical zone to an effective 4 seconds, compared to 7–10 seconds when using older generation laser platforms. Another feature to reduce treatment time is the advanced fluence level adjustment system, in which a mix of high and low fluence levels are used. High fluence level will perform 80% of corneal ablation, while low fluence will be used for fine correction, which improves resolution with remarkable precision in high refractive errors. Also, the reduction of induced aberrations is a critical trend in modern excimer laser refractive surgery. The latest generation platforms feature advanced ablation profiles, with the reduction of spot size being a key factor of control of the induced aberrations [24, 46, 76, 130].

The efficiency of an advanced ablation profile requires extremely accurate laser spot placement, in which the eye tracker latency time is of only 1.6 milliseconds (ms). A conventional laser platform eye tracker with a capturing rate of 60 to 330 Hz is able to detect the pupil position at 4000 Hz with a response time of 36 ms, which is clearly not fast enough for a high-speed laser platform of a speed reaching 700 Hz. The new five-dimensional turbo speed trackers have an acquisition speed of 1050 Hz generating a response rate of less than 3 ms with unique rotational balance, tracking both the pupil and the limbus. A conventional eye tracker adjusts eye movements into an X and Y-axis linear movement, and lasers are able to follow eye rolling, through translation of these linear movements into rotations with the help of an eye model, so that these generated rotations can be followed and compensated. Modern eye trackers do not only follow these horizontal and vertical displacements of the eye but also track the

cyclotorsional rotations. These cyclorotations can be classified into a static cyclorotation component, which occurs when the patients move from an upright to a supine position, and a dynamic cyclorotation component, which occurs during the procedure [3, 24].

The high repetition rate of excimer lasers may result in a shorter interval between laser pulses on the same area of the cornea, therefore, increasing the thermal load on the cornea and resulting in thermal damage. The latest generation lasers also use an intelligent thermal effect control to significantly reduce the heating effect on the cornea by blocking the area around an applied laser spot for a certain time allowing the cornea to cool down. This generates a dynamic thermally optimized distribution of the laser pulses, with enough time for each spot to cool down between pulses [24].

Another safety feature of the latest excimer laser platforms is the automatic monitoring of the pupil size, with the illumination being automatically adjusted in such a way that the pupil is exactly the same size at the start of the treatment as it was on the preoperative examination. Finally, the integrated online pachymetry (available on request only in one manufacturer's device) will display the corneal thickness in real time, with the ability to monitor the targeted measurements before and after flap lifting as well as during and after laser ablation, which is documented in the treatment log at the end of the procedure [24].

Advantages of FS-LASIK over other corneal refractive techniques

A major advantage of FS-LASIK is the very fast visual rehabilitation. In SMILE, on the other hand, a transient haze-like reaction and interface roughness can be clinically observed at a slit-lamp examination the first weeks after the procedure. Thus, the visual rehabilitation after might be prolonged compared to FS-LASIK. This corneal opacification and interface irregularities usually regress and become clinically insignificant 3 months after SMILE surgery [29, 48]. Similarly, the visual recovery in FS-LASIK is more rapid compared to PRK, without any postoperative pain or incidence of haze [114].

From a surgical perspective, FS-LASIK is admittedly a less challenging procedure compared to SMILE, which has a steeper learning curve. Moreover, FS-LASIK with the use sophisticated ablation profiles (e.g. topography-guided, wavefront-guided) as well as the use of latest eye-tracking technology with intraoperative control of centration and compensation of cyclotorsion, seems to result in better outcomes compared to SMILE, regarding refractive predictability and accuracy. It has also been reported that FS-LASIK may result in less induced HOA associated with decentration (e.g. vertical and/or horizontal coma), although this topic remains controversial in the published literature [16, 41, 143].

Complications and Challenges of FS-LASIK

Intraoperative complications in FS-LASIK include suction loss during flap creation (incomplete flap), flap-related complications, such as a free cap (absent hinge), buttonholes, oval/irregular/thin flap and flap displacement, decentration of the ablation zone and epithelial defects. Postoperative complications include interface complications such as infectious keratitis, diffuse lamellar keratitis, central toxic keratopathy, pressure-induced stromal keratopathy (interface fluid syndrome), epithelial ingrowth and foreign bodies at the interface (e.g. fibres). A very common postoperative complication is the dry eye. Also, flap complications, such as striae and folds as well as traumatic flap dislocation, may compromise the postoperative visual outcome. Moreover, monocular ghost images (associated with HOA), residual refractive error, regression of the refractive error and corneal neuralgia may occur. The most serious complication is the iatrogenic ectasia [2, 70, 95, 96, 106, 108, 129].

One of the main challenges during excimer laser procedures, such as the FS-LASIK is the ablation centration. Despite the great progress in eye-tracking technology, the issue of subclinical decentration of the ablation zone (< 1.0 mm) remains [14, 49, 74, 131]. The decentration of ablation can lead to undercorrection, irregular astigmatism and coma, with the effect of decentration being more prominent in hyperopic corrections. Moreover, FS-LASIK seems to induce a greater reduction of the corneal biomechanical strength compared to SMILE and PRK, which is mainly

associated with the flap cut and could lead to the development of iatrogenic ectasia [40, 96, 108, 136, 141]. Also, the increased PTA because of the flap cut enables, theoretically, the correction of smaller refractive errors compared to SMILE [96, 108].

Furthermore, in FS-LASIK, besides the photodisruptive effect of the femtosecond laser for the flap creation, the cornea is additionally burdened by the effect of the excimer laser. The tissue trauma following the excimer laser photoablation releases various cytokines and chemokines that modulate the corneal wound healing process and may induce inflammation. It has been shown that the expression of early inflammatory markers increased significantly when high-power corrections were performed and cornea reflectivity showed more intense and abundant light-scattering particles as a result of the photoablation process [48, 55, 104].

Another major issue after FS-LASIK is the dry eye. The pathophysiology of dry eye after LASIK is mainly associated with damage of the subepithelial nerve plexus and the stromal nerves as a result of the flap cut and the photoablation. The loss of conjunctival goblet cells, because of the suction used for flap creation by microkeratomes and femtosecond lasers, and the postoperative inflammatory changes may also contribute to post-LASIK dry eyes. Inflammation at or near the nerve endings may directly stimulate pain through either pressure or other direct action on the nerve. Alternatively, inflammation could exacerbate a pre-existing dry eye state, destabilizing the tear film through a cytokine-mediated reduction of tear film quality. Ocular surface dryness is known to be associated with chronic inflammation of the ocular surface, and the presence of inflammatory cytokines in the tear film and conjunctival epithelium. It is hypothesized that the inflamed postsurgical state could contribute to propagating inflammation on the ocular surface. Finally, the post-LASIK dry eye is associated with the change in corneal shape, which may affect the relationship between the eyelids and ocular surface and lead to abnormal tear distribution during blinking. A corneal iron line can sometimes be seen within the area of the LASIK flap, reflecting an alteration in the surface tear dynamics of the cornea [45, 115].

Regarding the induction of HOA, it has been shown that FS-LASIK induces more spherical aberrations, compared to SMILE. This effect, which is mainly associated with the ablation zone diameter as well as the flap cut, results in poorer visual quality with

halos, glare, ghost images and decreased contrast sensitivity, especially in low-light conditions. Although the use of aspheric ablation profiles has reduced the induction of spherical aberrations, the problem still remains [16, 41, 57, 60, 86, 123, 143]. Regarding the induction of coma, the results presented in the published literature by different research groups are controversial. A recent meta-analysis on the clinical outcomes after FS-LASIK and SMILE suggested no significant differences in the induced vertical and horizontal coma [140].

1.5.3 Centration of the treatment zone in SMILE versus FS-LASIK

Targeting at the Coaxially Sighted Corneal Light Reflex versus Entrance Pupil Centre

The centration of the treatment zone during corneal refractive procedures remains a topic of great dispute among refractive surgeons. Despite the benefits of a pupillary centration, it is widely accepted that a centration in regard to the visual axis is the key to optimized visual outcomes while maintaining the functional corneal morphology after the treatment [89, 101, 121, 132]. The advent of eye trackers led to a significant reduction of extended decentrations and therefore to fewer functional deficits, such as reduced corrected distance visual acuity, irregular astigmatism, halos, glare [27], reduced contrast sensitivity [128], and monocular diplopia [75]. However, despite the efficacy of laser treatments based on eye-tracking systems, the problems of subclinical decentrations (< 1.0 mm) and induction of HOA still remain [74].

Refractive lenticule extraction techniques, such as SMILE, and standard ablation profiles can effectively correct myopia and myopic astigmatism. However, the quality of vision in many cases could decrease substantially, especially under mesopic and low-contrast conditions, due to induction of HOA, even by subclinical decentrations as small as 0.2 mm [4, 68, 74]. Several researchers, including Uozato and Guyton back in 1987, supported the opinion that corneal refractive procedures should be centred at the EPC rather than the CSCLR [132]. Indeed, a centration targeted at the EPC allows the whole aperture of the eye's optical system to be covered with the ablation profile and minimizes the required optical zone [121, 132]. In addition, the EPC can be easily

located and tracked by eye-tracking systems. This could potentially eliminate the risk of extended decentrations or non-homogenous ablation patterns. However, the pupil centre is an unstable point which shifts with changes in pupil diameter, and the entrance pupil, used as reference point, is a virtual image of the real pupil as seen through the cornea [142]. Moreover, the efficacy of pupil tracking might be limited due to parallax error because eye tracker locates corneal positions by tracking the subjacent EPC [13, 93].

In contrast, the CSCLR provides a stable morphologic reference, which in cases of small or moderate angle K is considered a good approximation of the point where the visual axis intersects the cornea, offering the opportunity of maintaining the functional corneal morphology after surgery. Many studies have reported outcomes in favour of the centration at the CSCLR. Pande and Hillman proposed the CSCLR as the reference point for an ideal centration closest to the CV [89]. Arbelaez et al. showed no significant differences regarding the visual and refractive outcomes between CV and pupil centration [4]. Nevertheless, fewer HOA were induced after centring the refractive procedure on the CV. Kermani et al. reported a greater risk of decentered ablations and inducted HOA by hyperopic treatments centred on the line of sight. [43] CSCLR is increasingly regarded as the preferable reference point of centration regardless of the degree of angle K. Reinstein et al. presented in 2013 a major study comparing refractive outcomes, visual quality, and subjective night vision between two groups of eyes with small and large angle kappa after moderate to high hyperopic LASIK where the ablation was centred on the CSCLR. The results showed similar outcomes in both groups for all tested parameters, providing evidence that refractive corneal ablation should not be systematically aligned with the EPC [101]. A problem, however, that could arise by the centration on the CSCLR is that determining its exact location depends on the surgeon's eye dominance, the surgeon's eye balance, or the stereopsis angle of the microscope [4, 19].

1.5.4 Intraoperative Alignment in SMILE and FS-LASIK

In all-in-one femtosecond laser procedures like SMILE, the alignment of the photodisruption is subjective and relies entirely on the patient, who must fixate on a

blinking light during the suction process and during the initial stage of the laser scan (after the laser cut of the lenticule's posterior plane, the blinking target is obscured by intracorneal gas bubbles). The surgeon controls and encourages the patient to maintain fixation in particular when the patient's view is obscured by intrastromal gas bubbles during the second half of the laser procedure in order to avoid suction loss. In SMILE for myopia correction, the centration is targeted at the corneal vertex (CV), which is identified by the coaxially sighted corneal light reflex (CSCLR) or the first image of Purkinje. [49, 52, 112]

The intraoperative alignment of the photoablation in myopic FS-LASIK is controlled by an active eye tracker. In the present study, the photoablation in the FS-LASIK group was performed with the MEL 80 excimer laser. The platform utilizes a 1,000-Hz eye tracker, which provides a 4:1 tracking-frame-to-pulse ratio, resulting in an extremely low full-loop delay between 2 and 4 milliseconds. An infrared light source illuminates the eye. The light reflects off the retina and illuminates the pupil. The eye tracker locates the EPC and the CSCLR. It also includes a cyclotorsion registration system that identifies the pupil, iris, limbus, and conjunctival vessels. It also allows manual centration by direct visualization of the position of the red helium-neon laser aiming beam so that it is simple to centre the ablation on the corneal reflex of a coaxially fixating eye. For the purposes of the present study, the alignment of the photoablation was targeted in all cases at the EPC [17, 54, 78, 83, 103, 127].

Angle Kappa

A very important issue regarding the achieved centration is its pattern in regard to the visual axis. The visual axis is the line which connects the fovea with the fixation point via the nodal point of the eye. The line of sight is defined as the line connecting the fixation point with the centre of the entrance pupil. The pupillary axis is the line passing through the EPC perpendicular to the cornea. The definition of angle kappa (angle K) is the angular distance between visual and pupillary axis [7, 90, 125], which is in myopic eyes approximately 2.0° and is mostly positive [90, 135]. As a result of positive angle K the first image of Purkinje is located nasal to the pupillary centre or

temporal in cases of a negative angle K. Studies conducted in order to assess the distribution of angle K in myopic eyes showed a prevalence of positive angle K in the majority of the tested subjects, while a negative angle K or no angle K was identified in substantially fewer cases (**Fig. 3**) [90, 109].

The issue of centration in SMILE, FS-LASIK and other corneal refractive procedures for myopia correction is considered to be less critical for the postoperative quality of vision compared to hyperopic treatments. In hyperopic eyes, the angle K is larger and the location of CSCLR may drift significantly from the location of the point where the visual axis intersects the cornea. Due to the small or moderate degree of angle K in myopic eyes, and the larger optical zone of the treated areas, centring the procedure on the CSCLR results on similar refractive and visual outcomes as targeting the intraoperative alignment at the EPC. Nevertheless, the goal in refractive surgery is the optimisation of the predictability of the refractive outcomes as well as the optimisation of the postoperative quality of vision. By evaluating and constantly improving the methods of intraoperative centration and determining the patterns of the achieved centration we would enable more accurate results, better quality of vision and better patient satisfaction.

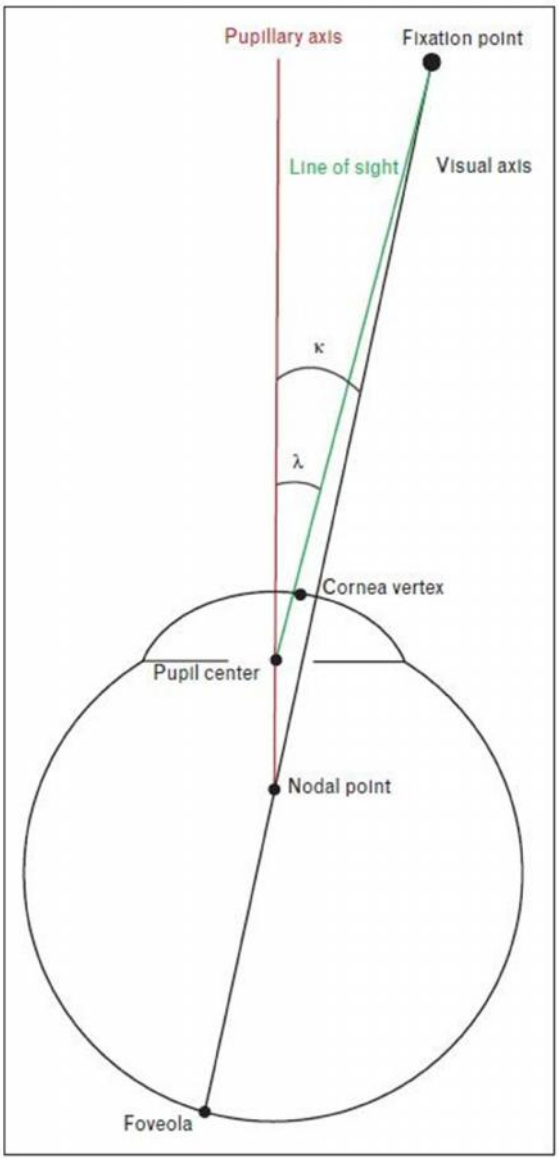

Fig. 3 Definition of angle lambda (λ), angle kappa (κ) and axes. Angle lambda represents the angle between the pupillary axis and the line of sight. Angle kappa represents the angle between the pupillary axis and the visual axis. Source [90]

Purpose

An argument often expressed by refractive surgeons is that a precise centration cannot be guaranteed in SMILE due to the subjective alignment and lack of eye tracking. Therefore, the purpose of the present study is to investigate and compare the centration of the treatment zone between eyes treated with SMILE and FS-LASIK, by using the CSCLR and the EPC as reference points on the differential pachymetry map of Pentacam, and evaluate the predictability of the intraoperative alignment. Moreover, the study aims in evaluating the pattern of the achieved centration in relation to the EPC and compare this pattern to the preoperative pattern of angle K i.e. the pattern of the preoperative CSCLR in relation to the EPC.

Methods

2.0 Subjects

For the present study, the data were obtained from 69 myopic eyes (34 right eyes and 35 left eyes) of 36 patients (16 male subjects and 20 female subjects) who underwent SMILE between July 2012 and February 2013. The FS-LASIK group included 69 myopic eyes (33 right eyes and 36 left eyes) of 36 patients (16 male subjects and 20 female subjects). All surgeries were performed by the same surgeon (Walter Sekundo) at the Department of Ophthalmology, Philipps University of Marburg. The procedures were performed using VisuMax® platform consisting of VisuMax femtosecond laser and MEL-80® excimer-laser (Carl Zeiss Meditec AG, Jena, Germany). Both techniques were performed under the same illumination conditions. The illuminance as measured with the Precision Gold N76CC Luxmeter under the femtosecond laser and under the excimer laser was 6 lux.

The standard protocol of preoperative evaluation for corneal refractive surgery included review and update of the patient's medical records, autorefraction, pupillometry, uncorrected distance visual acuity (UDVA), corrected distance visual acuity (CDVA), manifest and cycloplegic refraction, slit-lamp examination of the cornea, the anterior segment and the retina, measurement of the intraocular pressure with a non-contact tonometer, tear film testing (Schirmer II, break up time), IOL-Master 500 (Carl Zeiss Meditec AG/Germany) biometry, wavefront aberrometry (WASCA-Carl Zeiss Meditec AG/Germany) and finally corneal topography and pachymetry using Pentacam. The same measurements were performed 1 month and 3 months postoperatively with the exception of IOL-Master biometry and cycloplegic refraction unless needed. Regarding the topographic and pachymetric analysis, we compared the preoperative measurements to the 3 month-postoperative measurements. Intraoperative parameters, such as the spherical equivalent (SE) of the correction, cylinder of the correction, cap/flap thickness, cap/flap diameter, lenticule

thickness/ablation depth, and lenticule/ablation diameter were also evaluated and compared.

The enrolling criteria included a stable refraction 2 years prior to surgery and a normal preoperative corneal topography. The exclusion criteria included any optical opacities or pathology detected during slit-lamp examination, previous corneal surgeries, ocular trauma or intraocular surgery, severe dry eye, corneal disease or ocular infection (e.g. herpes simplex virus, herpes zoster ophthalmicus), collagen vascular/autoimmune diseases (e.g. systemic lupus erythematosus, Sjogren's syndrome, rheumatoid arthritis). All patients provided and informed consent for the surgery, acknowledging potentials intraoperative and postoperative complications and risks of the procedure.

2.1 Description of the Procedures

Both techniques were performed under the same illumination conditions. The illuminance as measured with the Precision Gold N76CC Luxmeter under the VisuMax femtosecond laser and under the MEL 80 excimer laser was 6 lux.

Small Incision Lenticule Extraction Surgical Protocol

All SMILE procedures were performed after application of topical anaesthesia. First, the skin of the periocular area was scrubbed. Then the eyelids and eyelashes were draped and a sterile eyelid speculum was inserted. The intrastromal refractive lenticules were created using the VisuMax femtosecond laser. The energy was set at 160nJ with a spot/track spacing of 4.5 μm for the horizontal plane and 2 μm for the sidecut. An entering incision between 2.5 and 4mm, depending on location and orbital features, was pre-cut by the laser. The lenticule side cut thickness was set to 15 μm. During the docking, the patient must fixate on a blinking green light. The fixation light shifts during the applanation of the cornea by the suction contact glass, but the patient is instructed not to move the eyes, especially when the suction is applied, in order to avoid

suction loss. The surgeon controls whether the patient maintains the fixation in particular when the patient's view is obscured by intrastromal gas bubbles during the second half of the laser procedure. In SMILE, the centration is targeted at the CSCLR. The laser performs first the posterior plane cut (refractive plane) in a spiral-in pattern, followed by the lenticule edge cut. Afterwards, the anterior plane is cut in a spiral-out pattern, followed by the entrance wound cut (**Fig. 4**). A Sinskey-like hook is used to break the entrance wound open and enter the incision. A small pocket (1 × 2 mm) is made at the anterior plane with the hook, followed by a small pocket at the posterior plane (at the opposite edge of the incision). The lenticule dissector is then entered inside the pocket at the anterior plane and dissects the tissue bridges at the anterior plane, first in the central area and then at the periphery. Afterwards, the posterior plane is dissected in a similar fashion. The lenticule in then removed using advanced lenticule forceps, although its removal may be accomplished with the use of the dissector (**Fig. 5**). After its removal, the lenticule is carefully inspected on the cornea surface and once confirmed as being whole, the pocket is flushed with BSS in order to remove any remained interface debris (cellular constituents, foreign bodies, epithelial cells). Finally, the peripheral incision and the corneal surface are gently wiped using a spear sponge soaked in BSS, and the interface is checked using a built-in slit lamp. After removing the speculum, antibiotic and steroid drops were applied. In general, the entire length of the SMILE procedure is about the half of the FS-LASIK. In bilateral cases, while the first eye is receiving the laser treatment, the second eye should be held shut with an adhesive strip, to prevent uneven dehydration of the epithelium that may lead to a temporary roughness of the surface, in turn affecting the smoothness of the laser cuts and the visual recovery time. Standard postoperative treatment was fluoroquinolone and dexamethasone eye drops four times daily for a week. The drops were slowly tapered off over a 4-week period. Preservative-free artificial tears five times a day were also prescribed for at least the first postoperative month [15].

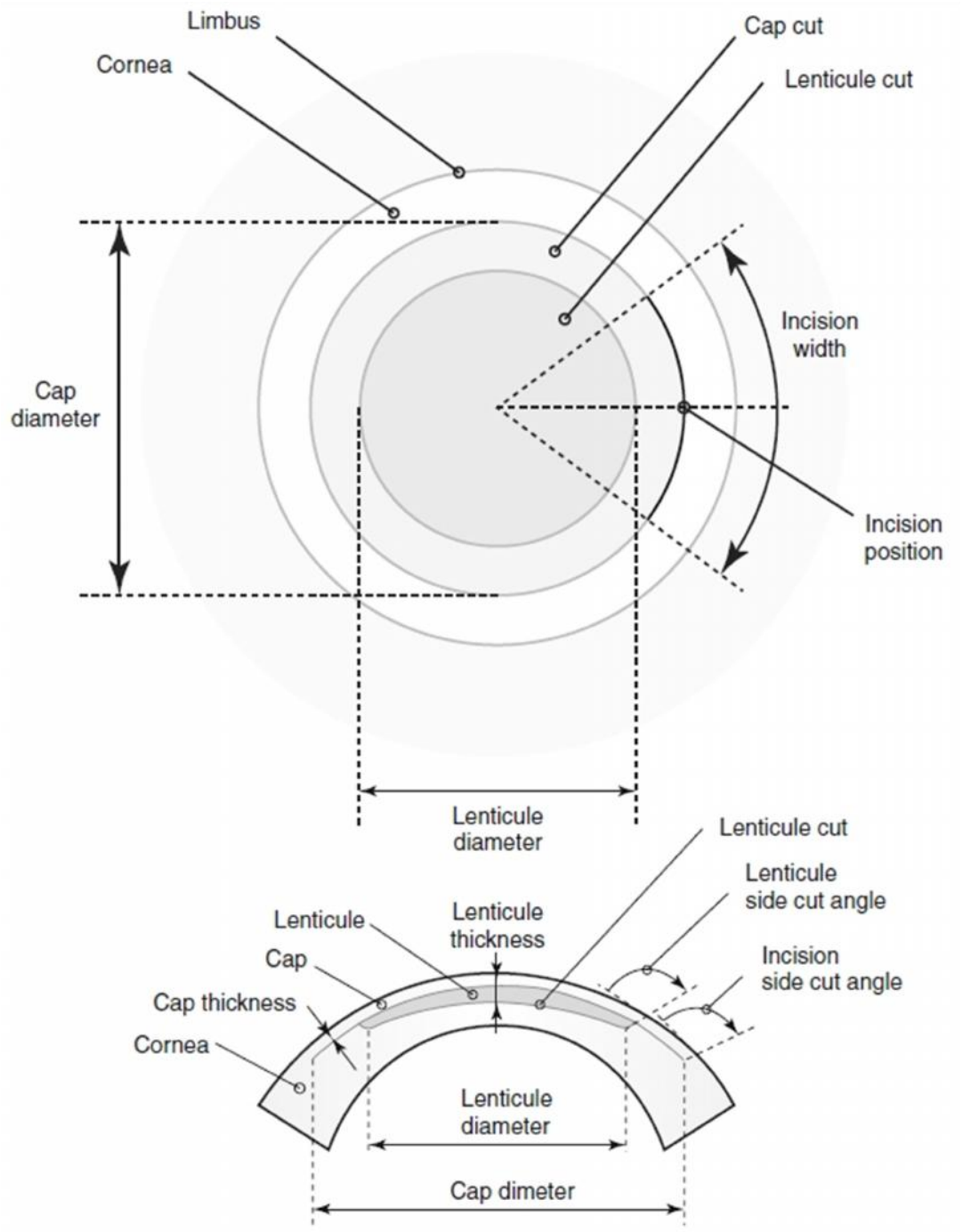

Fig. 4 Parameters associated with SMILE for myopia. The first picture is a schematic view of the cornea from above with lenticule and cap already cut. The second picture is the side view the cornea with lenticule and cap already cut. Source [9]

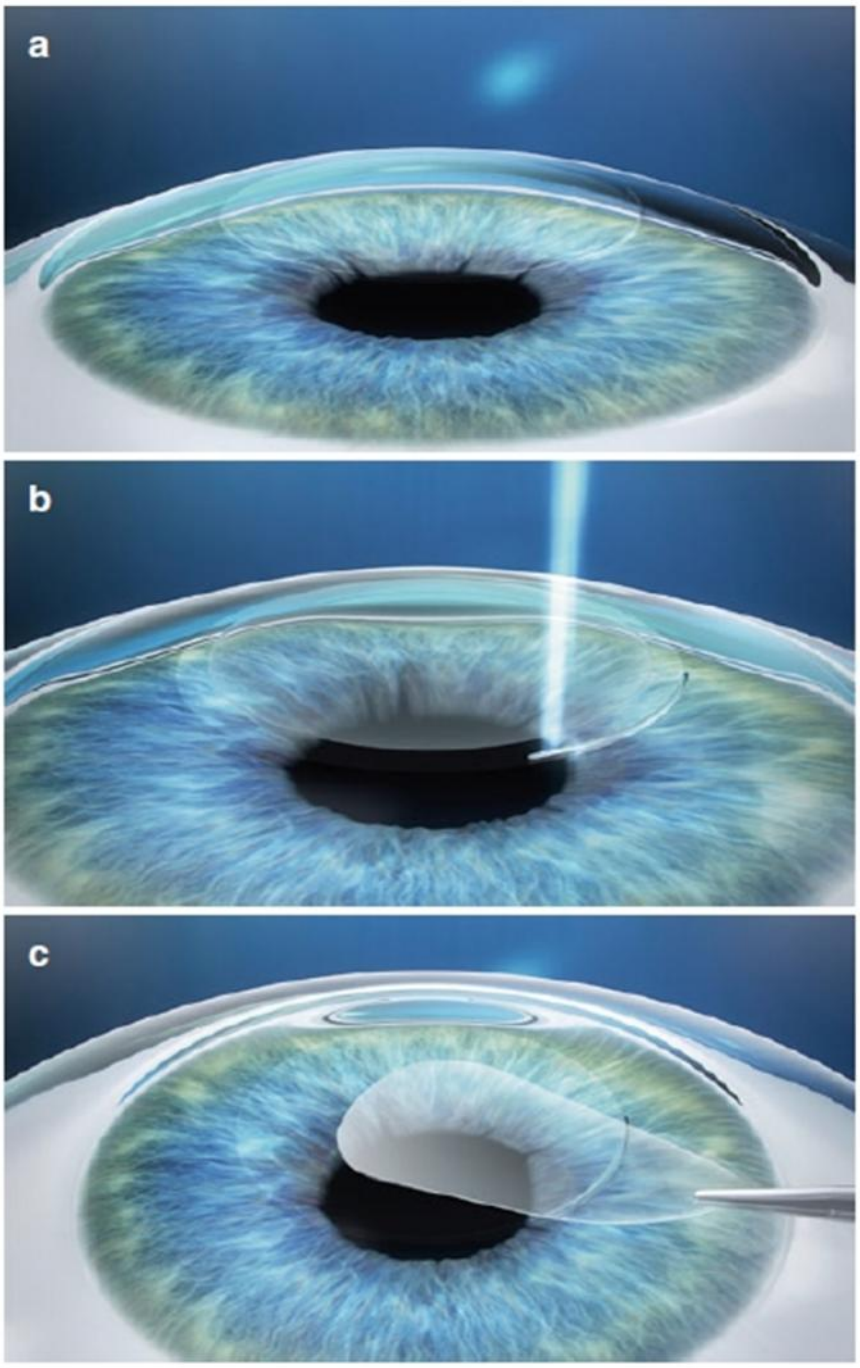

Fig. 5 A schematic drawing of the SMILE procedure. The VisuMax femtosecond laser system (a) cuts the lenticule followed by a (b) small incision. The lenticule is removed through the (c) small incision. Source [10]

Femtosecond laser-assisted LASIK Surgical Protocol

All FS-LASIK procedures were performed after application of topical anaesthesia. First, the skin of the periocular area was scrubbed. Then the eyelids and eyelashes were draped and a sterile eyelid speculum was inserted. The flaps were created using the VisuMax femtosecond laser. Similarly to SMILE, the energy was set between 160 and 180nJ with a spot/track spacing of 4.5 μm for the horizontal plane and 2 μm for the sidecut. During the docking process, the patient was asked to observe the green blinking fixation light under dim surrounding illumination and the suction was initiated. The laser performed the flap cut in spiral-in pattern with a superior hinge (**Fig. 6**). After both flaps (right eye followed by left eye) were pre-cut the patient was rotated on the same bed under the MEL 80 excimer laser. Here, the periocular area was draped with sterile plastic foil and a suction speculum, connected to a pump, was inserted. A Sinskey-like hook was used to create a small incision along the furrow of the flap side cut near the hinge. Afterwards, a Seibel flap lifter (Rhein Medical Inc., Tampa, FL, USA.) was inserted under the flap edge through the incision, dissected the remaining tissue bridges, and the flap was finally lifted. The cornea bed was flushed with BSS and the patient asked to look at the green blinking light, while the surrounding illumination was turned down. The eye-tracker was logged onto the EPC and the ablation started (**Fig. 7**). After the ablation was completed, the flap was repositioned and the interface was flushed with BSS. The flap surface was wiped and stretched with sponges. All eyes were carefully inspected for proper flap alignment as well as uniformity of the gutter in order to avoid flap striae. After carefully removing the speculum, antibiotic and steroid drops were applied. The patient was then rotated back under VisuMax and the flaps, as well as the interface, were examined using a built-in slit lamp of the femtosecond laser. Standard postoperative treatment was fluoroquinolone and dexamethasone eye drops four times daily for a week. The drops were slowly tapered off over a 4-week period. Preservative-free artificial tears five times a day were also prescribed for at least the first postoperative month.

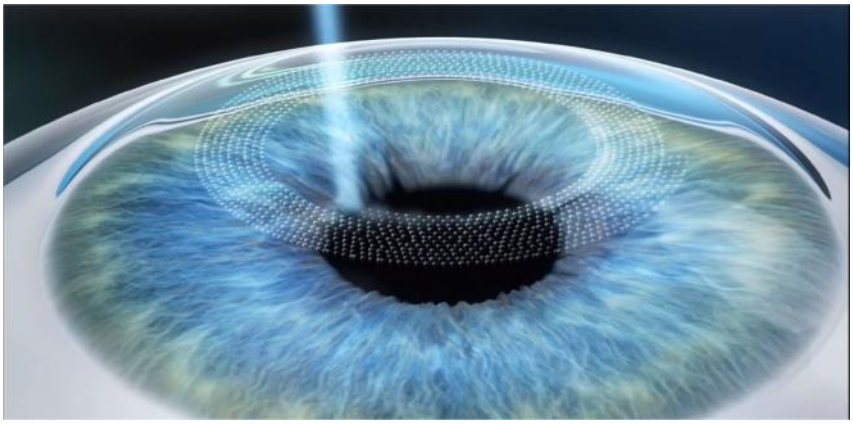

Fig. 6 Femtosecond laser-assisted flap creation (spiral-in pattern). Source https://www.zeiss.com

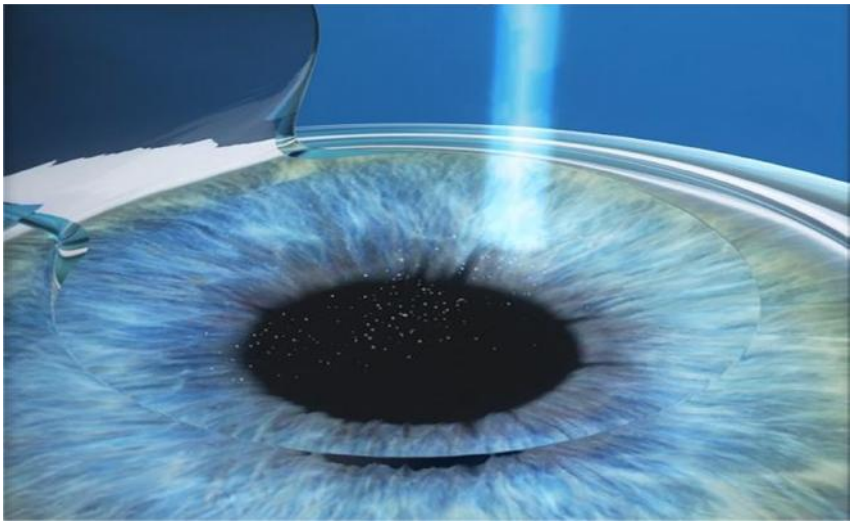

Fig. 7 After the flap is lifted, the excimer laser reshapes the stromal bed. Source https://www.zeiss.com

2.2 Method of Centration Analysis and Angle K Evaluation

For the purposes of the present study, the degree of angle K was estimated indirectly by the coordinates of the CV on the preoperative pachymetry maps of Pentacam. When the patient fixates on the red spot, in the middle of the monochromatic slit light source (blue LED at 475 nm), then the reference axis of the instrument (measurement axis) and the patient's visual axis would be coaxial. In this case, the intercept of the instrument's reference axis and the cornea would be the CV [66, 90]. This point is called corneal apex (CA) in the Pentacam software, which is a misnomer for vertex, as the CA should academically refer to the point of greatest corneal curvature or shortest radius [66, 90, 139] (**Fig. 8**). Knowing the location of the CV, we can estimate the location of the preoperative CSCLR and also evaluate the angle K, because the CSCLR is a good approximation of the point where the visual axis intersects the cornea.

The centration of the photodisruption zone in SMILE and the photoablation zone in FS-LASIK was evaluated on the pachymetry differential maps of Pentacam. The point of maximum pachymetric difference (PMPD), which corresponds to the maximum refractive power and the centre of mass of the lenticule or the photoablated tissue, was located on the pachymetry differential maps. In several cases, there was more than one point corresponding to the maximum pachymetric difference. For that reason, three consecutive measurements were performed by the same observer (Apostolos Lazaridis) on each eye and the average coordinates of these measurements were calculated. Then, the distance of the PMPD from the topographical EPC and from the CA was calculated (based on the coordinates of each point, which are provided by Pentacam) using the Pythagorean Theorem (**Fig. 9**). The coordinates of the EPC and the CA on the differential maps are the same as on the preoperative maps. That allowed us to evaluate the centration in relation to the preoperative corneal parameters, and therefore avoid misguided measurements related to EPC or CA shift, which might be observed at the postoperative maps due to changes in pupil diameter and changes in corneal morphology, respectively. All measurements were conducted under the same

illumination conditions. In order to avoid misleading calculations due to a shift of the EPC because of changes in the dilation of the pupil, the lighting conditions in the Pentacam room were adjusted so that the illuminance in front of the Pentacam would be the same as the illuminance under the femtosecond laser and the excimer laser. The illuminance in front of Pentacam as measured with the Precision Gold N76CC Luxmeter was 6 lux.

2.3 Statistical Analysis

Descriptive statistics (i.e., mean, standard deviation, minimum, maximum, and range) were performed using Microsoft Excel 2010 (Microsoft Corporation, Redmond, WA). Statistical analysis was performed using SPSS version 19.0 (SPSS Inc., Chicago, IL). The normality of the distribution of all examined variables was evaluated with Shapiro-Wilk test. Comparisons within each group were performed using the Student's t-test or Wilcoxon signed-rank test, according to the normality of data distribution. Comparisons between the two groups were performed using unpaired t-test or Mann-Whitney U test, according to normality of data distribution. Fisher's exact test was used for statistical analysis of nominal variables. All parametric and non-parametric tests were performed at the level of significance of 95%. P values less than 0.05 were considered statistically significant. All preoperative and postoperative data used in the present study derived from the patients' medical records, the Pentacam files, and the VisuMax files, at the Department of Ophthalmology, Philipps University of Marburg.

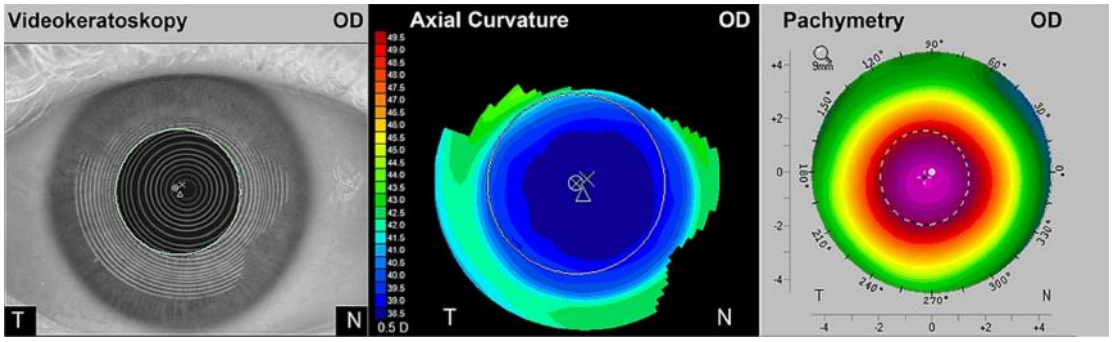

Fig. 8 Corneal landmarks as being identified by Altas (Carl Zeiss Meditec AG, Germany) and Pentacam (Oculus GmbH, Germany) for the same patient. The first two images (videokeratoskopy and axial curvature) were created by Atlas. The corneal vertex (CV) is depicted with an X, the entrance pupil centre (EPC) with ⊗ and the corneal apex (CA) with ∆. The last image represents a postoperative pachymetry map of Pentacam. The EPC is depicted with a cross, the pupil edge with a white dotted circle and the CA with a white dot. Note that the point identified as CA by Pentacam has the same displacement in relation to the EPC as the CV on Atlas images. This example further supports the assumption that the CA in Pentacam software is actually the CV. Source [52].

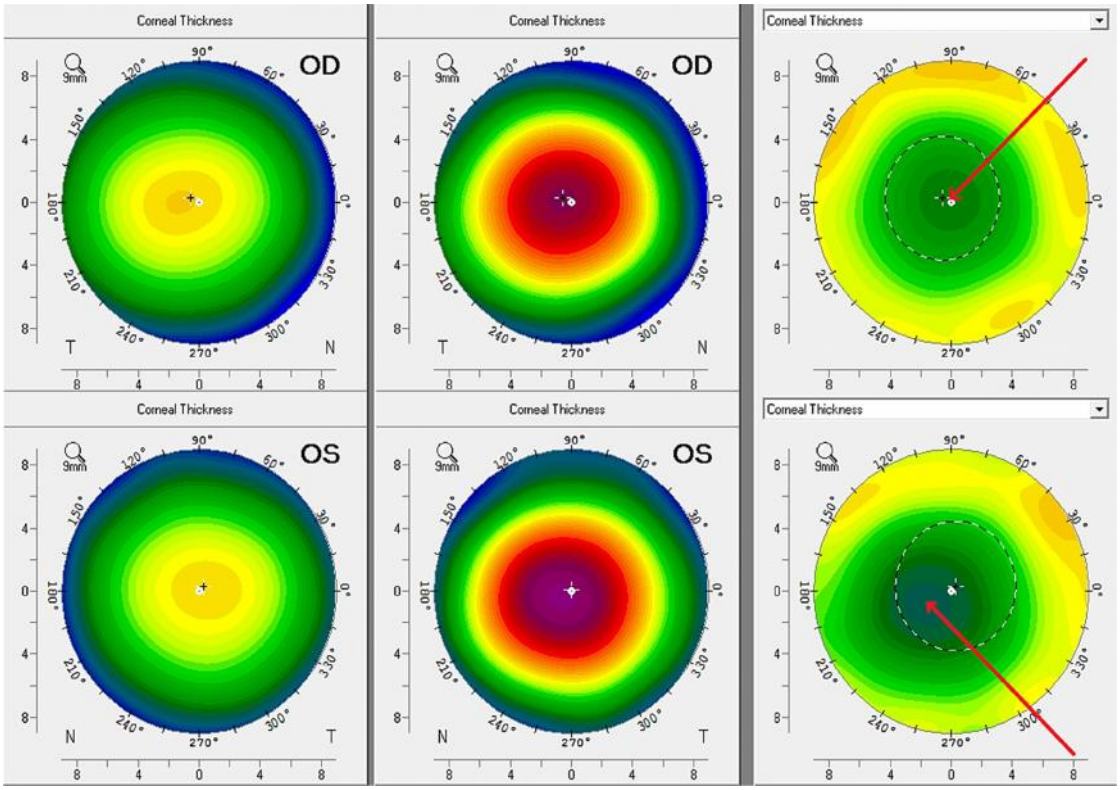

Fig. 9 SMILE case - Pachymetry maps of the same patient preoperative, 3 months postoperative and differential pachymetry maps. The EPC is depicted with a cross, the pupil edge with a white dotted circle and the CA with a white dot. The red arrow shows the point of the maximum pachymetric difference. **OD:** well centred lenticule zone (distance of the thickest point from CA: 0.103 mm, distance of the thickest point from EPC: 0,243 mm **OS:** decentered lenticule zone (distance of the thickest point from CA: 0.863 mm, distance of the thickest point from EPC: 1.062 mm). Source [49]

RESULTS

3.0 Analysis of the Preoperative Variables

In SMILE group, the mean value and standard deviation of the age of the patients were 38 ± 10 years, ranging from 22 to 55 years. Fifty-one eyes underwent full correction of the refractive error and 18 were primarily undercorrected. The mean value and standard deviation of the SEQ of the preoperative refraction was -5.96 ± 1.9 D, ranging from -1.25 to -10 D. The mean value and standard deviation of the cylinder of the preoperative refraction was -0.95 ± 1.0 D of cylinder, ranging from 0 to -4.0 D. The mean value and standard deviation of the central simulated keratometer readings (n=1.3375) was 43.53 ± 1.51, ranging from 40.2 to 46.8 D (**Table 1**).

In FS-LASIK group, the mean value and standard deviation of the age of the patients were 34 ± 11 years, ranging from 23 to 65 years. Sixty-three eyes received full correction of the refractive error and 6 were primarily undercorrected. The mean value and standard deviation of the SEQ of the preoperative refraction was -4.96 ± 2.43 D, ranging from -0.75 to -10 D. The mean value and standard deviation of the cylinder of the preoperative refraction was -1 ± 1.04 D of cylinder, ranging from 0 to -4.5 D. The mean value and standard deviation of the central simulated keratometer readings (n=1.3375) was 43.43 ± 1.35 D, ranging from 40.2 to 46.6 D (**Table 1**).

Comparison of the quantitative variables between the two groups showed no statistically significant differences of preoperative SEQ, cylinder and central simulated keratometer readings ($P \geq 0.09$) (**Table 1**).

Table 1. Demographics and preoperative refractive data

Variables	**SMILE**	**FS-LASIK**	***P***
Patients	36	36	-
Total Eyes (Right/Left)	34/35	33/36	-
Gender (M/F)	16/20	16/20	-
Mean Age (y)	38 ± 10 (22 to 55)	34 ± 11 (23 to 65)	0.030
Mean SEQ (D)	-5.96 ± 1.9 (-10 to -1.25)	-4.96 ± 2.43 (-10 to -0.75)	0.090
Mean Cylinder (D)	-0.95 ± 1.0 (-4.0 to 0)	-1 ± 1.04 (-4.5 to 0)	0.798
Mean central Simulated Keratometer readings (D)	43.53 ± 1.51 (40.2 to 46.8)	43.43 ± 1.35 (40.2 to 46.6)	0.614

3.1 Analysis of the Intraoperative Variables

In SMILE group, the mean value and standard deviation of the SEQ of the correction (data entered in VisuMax) were -5.70 ± 1.95 D, ranging from -1.25 to -10 D. The mean value and standard deviation of the cylinder of the correction were -0.79 ± 1.04 D of cylinder, ranging from 0 to -4.0 D. The mean value and standard deviation of the cap thickness were 118 ± 3.8 μm, ranging from 100 to 120 μm. The mean value and standard deviation of the cap diameter were 7.8 ± 0.1 mm, ranging from 7.5 to 8.0 mm. The mean value and standard deviation of the lenticule thickness were 120 ± 27 μm, ranging from 48 to 164 μm. The mean value and standard deviation of the diameter of the lenticule were 6.7 ± 0.2 mm, ranging from 6.2 to 7.0 mm (**Table 2**).

In FS-LASIK group, the mean value and standard deviation of the SEQ of the correction (data entered in MEL-80) were -4.80 ± 2.5 D, ranging from -0.75 to -10 D. The mean value and standard deviation of the cylinder of the correction were -0.91 ± 1.07 D of cylinder, ranging from 0 to -4.5 D. The mean value and standard deviation of the flap thickness were 114 ± 5.4 μm, ranging from 100 to 120 μm. The mean value and standard deviation of the flap diameter were 8.36 ± 0.1 mm, ranging from 8.0 to 8.5 mm. The mean value and standard deviation of the ablation depth were 120 ± 27 μm, ranging from 48 to 164 μm. The mean value and standard deviation of the diameter of the ablation were 6.32 ± 0.2 mm, ranging from 6.0 to 6.75 mm (**Table 2**).

Comparison of the above-described variables showed statistically significant differences between the two groups regarding the SEQ and the cylinder of the correction, the cap/flap thickness, the cap/flap diameter, and the lenticule thickness/ablation depth ($P \leq 0.038$) (**Table 2**). The significant differences between the two groups for the aforementioned surgical variables do not induce any bias in the evaluation of the main examined parameters of the study.

Table 2. Surgical data

Variables	SMILE	FS-LASIK	*P*
Mean SEQ of the correction (D)	-5.70 ± 1.95 (-10 to -1.25)	-4.80 ± 2.5 (-0.75 to -10)	0.038
Mean Cylinder of the correction (D)	-0.79 ± 1.04 (-4.0 to 0)	-0.91 ± 1.07 (-4.5 to 0)	0.000
Mean Flap/Cap Thickness (μm)	118 ± 3.8 (100 to 120)	114 ± 5.4 (100 to 120)	0.000
Mean Flap/Cap Diameter (mm)	7.8 ± 0.1 (7.5 to 8.0)	8.36 ± 0.1 (8.0 to 8.5)	0.000
Mean Lenticule Thickness/ Ablation Depth (μm)	120 ± 27 (48 to 164)	103 ± 37 (22 to 165)	0.067
Mean Lenticule/ Ablation Diameter (mm)	6.7 ± 0.2 (6.2 to 7.0)	6.32± 0.2 (6 to 6.75)	0.000

3.2 Analysis of preoperative Angle K

The points of the preoperative CSCLR of both groups are depicted in **Fig 10A** and **10B**. For right eyes (blue dots), the points with positive x-coordinates correspond to positive angle K, whereas the points having negative x-coordinates correspond to negative angle K. For left eyes (red dots), the points with negative x-coordinates correspond to positive angle K, whereas the points with positive x-coordinates correspond to negative angle K. When the points were on the y-axis (0, y), the angle K was 0°.

By evaluating the angle K according to the location of the preoperative CSCLR, in the SMILE group, there were 32 right eyes and 24 left eyes with positive angle K, 2 right eyes and 11 left eyes with negative angle K, and no eyes with 0° angle K (**Table 3**). In the FS-LASIK group, there were 29 right eyes and 22 left eyes with positive angle K, 3 right eyes and 14 left eyes with negative angle K, and 1 right eye with 0° angle K (**Table 3**).

In both groups, the location of the preoperative CSCLR demonstrated a nasalization pattern since angle K was positive in most eyes (**Fig 10A** and **10B**). In SMILE group, the mean distance of the point corresponding to the preoperative CSCLR from the EPC was 0.227 ± 0.121 mm, ranging from 0.014 to 0.602 mm. In FS-LASIK group, this distance was 0.206 ± 0.097 mm, ranging from 0.045 to 0.457 mm. Statistical analysis showed no significant difference between the two groups (P=0.201), suggesting that there would also be no significant difference between the two groups regarding the mean angle K. (**Table 3**).

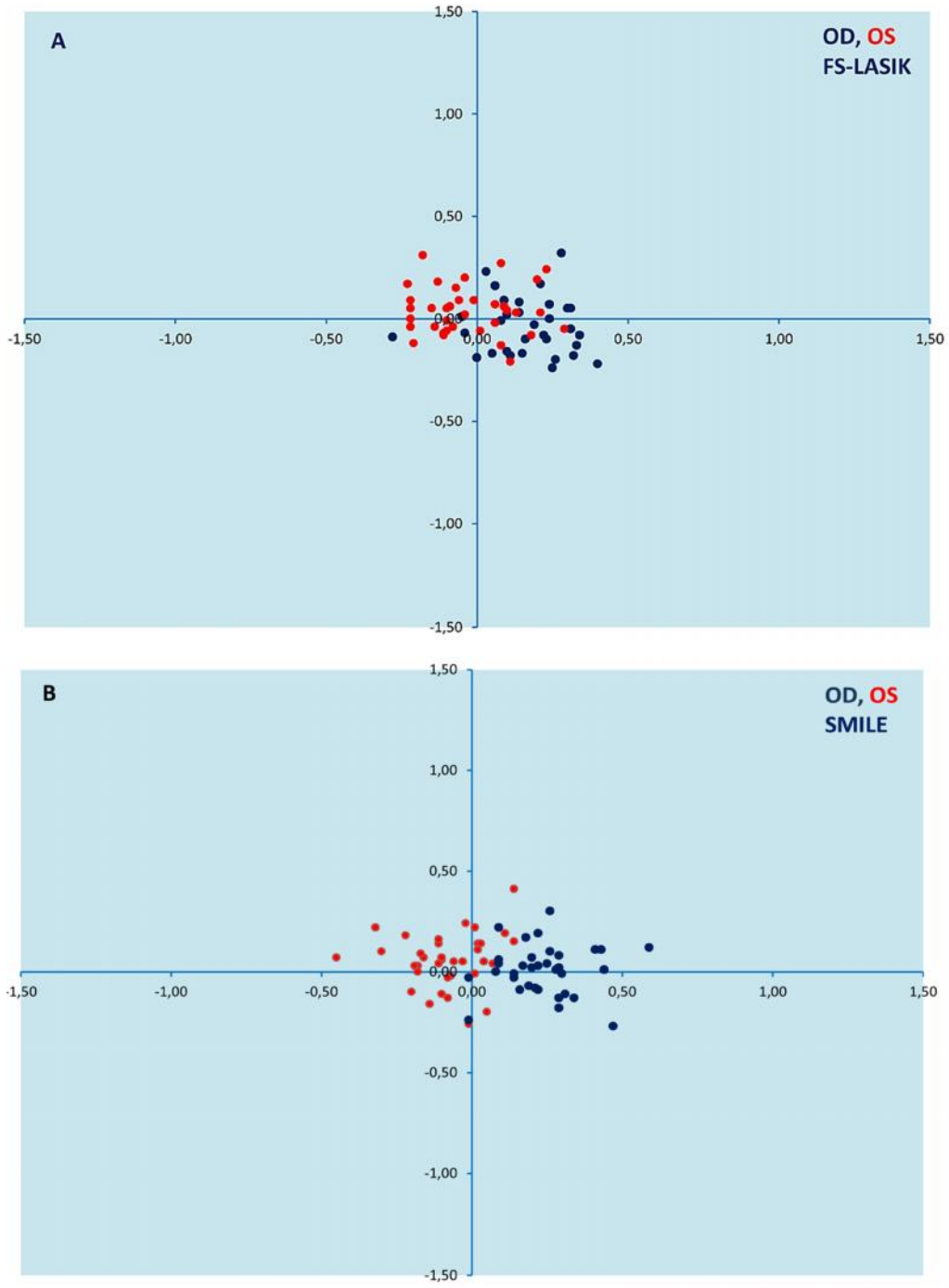

Fig. 10 (A) FS-LASIK group. Depiction of the points of the preoperative CSCLR in relation to the EPC (0,0). (B) SMILE group. Depiction of the points of the preoperative CSCLR (attempted centration) in relation to the EPC (0,0). Source [49, 52]

Table 3. Angle K

		SMILE			FS-LASIK			*P*
Mean Distance of preoperative CSCLR from EPC		0.227 ± 0.121 (0.014 to 0.602)			0.206 ± 0.097 (0.045 to 0.457)			0.201
Preoperative Pattern of angle K (no. of eyes)		**pos**	**neg**	**none**	**pos**	**neg**	**none**	-
	OD	32	2	0	29	3	1	
	OS	24	11	0	22	14	0	
	Total	56	13	0	51	17	1	

3.3 Analysis of Centration Data - Attempted versus Achieved Centration

In SMILE group, the eccentricity of the treatment zone was estimated by the distance between the PMPD (achieved centration) and the preoperative CSCLR (attempted centration in SMILE; the CSCLR, which is represented in the Pentacam software by the coordinates of the apex) and was 0.315 ± 0.211 mm, ranging from 0.0 to 1.131 mm (**Table 4**).

In FS-LASIK group, the eccentricity of the treatment zone was estimated by the distance between the PMPD (achieved centration) and the preoperative EPC (attempted centration in FS-LASIK) and was 0.452 ± 0.224 mm, ranging from 0.02 mm to 1.040 mm (**Table 5**).

The comparison between the two groups showed a statistically significant difference regarding the decentration of the treatment zone from the reference point of centration for each technique, with the decentration being more extended in FS-LASIK ($P < .001$).

In order to assess the incidence of small (0 - 0.2 mm), moderate (0.2 - 0.5 mm) and high (0.5 - 1 mm or >1 mm) decentrations, we measured the extent of decentration of the PMPD from the reference point of its technique. As shown in **Fig. 11** there are substantially more SMILE eyes with small, subclinical decentrations up to 0.2 mm. Both techniques show a similar incidence of moderate decentrations (0.2 - 0.5 mm). Regarding the high decentrations (0.5 - 1 mm or >1 mm) we observe that there are more FS-LASIK eyes with highly decentered ablation profiles.

Bringing together the various PMPD of each patient on a Cartesian coordinate system and marking the right eyes with blue colour and the left eyes with red, we managed to visualize the attempted and the achieved centration for the two groups. In FS-LASIK group the achieved centration of each eye is depicted in **Fig 12A**. As we observe, the points corresponding to the centres of the photoablated tissue in relation to the EPC are quite dispersed. The achieved centration of each eye in the SMILE group is depicted in **Fig 12B**. As we observe, the points corresponding to the centres of the

lenticules in relation to the CSCLR are more accumulated around the target point compared to FS-LASIK and this is also verified from our measurements (**Table 4 & 5**).

Table 4. Decentration and pattern of the achieved centration in SMILE

SMILE		
Decentration from the reference point of attempted centration Mean Distance between PMPD and preoperative CSCLR (mm)		0.315 ± 0.211 (0.0 to 1.131)
Mean Distance between PMPD and the EPC (mm)		0.326 ± 0.196 (0.014 to 1.062)
Achieved centration following the preoperative pattern of angle K	**OD**	26/34 (76.47%)
	OS	26/35 (74.28%)
	Total	52/69 (75.36%)

Table 5. Decentration and pattern of the achieved centration in FS-LASIK

FS-LASIK		
Mean Distance between PMPD and preoperative CSCLR (mm)		0.516 ± 0.254 (0.103 to 1.265)
Decentration from the reference point of attempted centration Mean Distance between PMPD and the EPC (mm)		0.452 ± 0.224 (0.02 to 1.040)
Achieved centration following the preoperative pattern of angle K	**OD**	14/33 (42.42%)
	OS	18/36 (50.00%)
	Total	32/69 (46.37%)

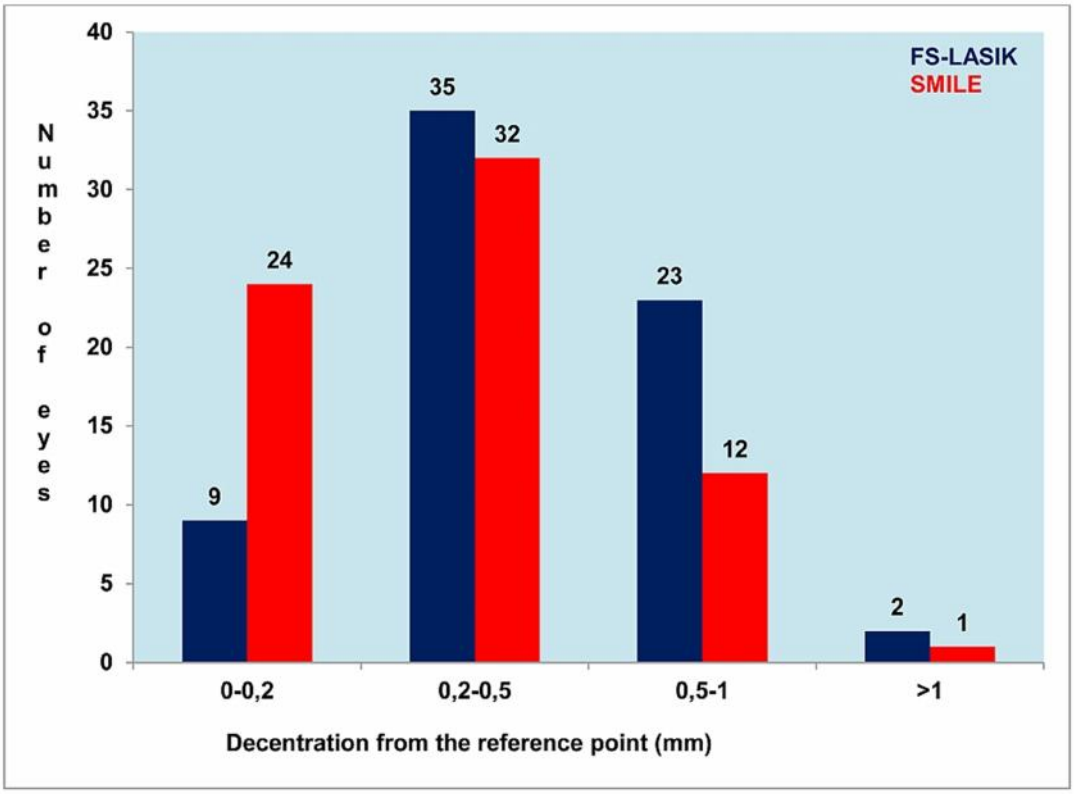

Fig. 11 Histogram of the distance of the PMPD from the reference point of its technique (mm). SMILE cases are presented with red columns and FS-LASIK cases with blue columns. Source [49, 52]

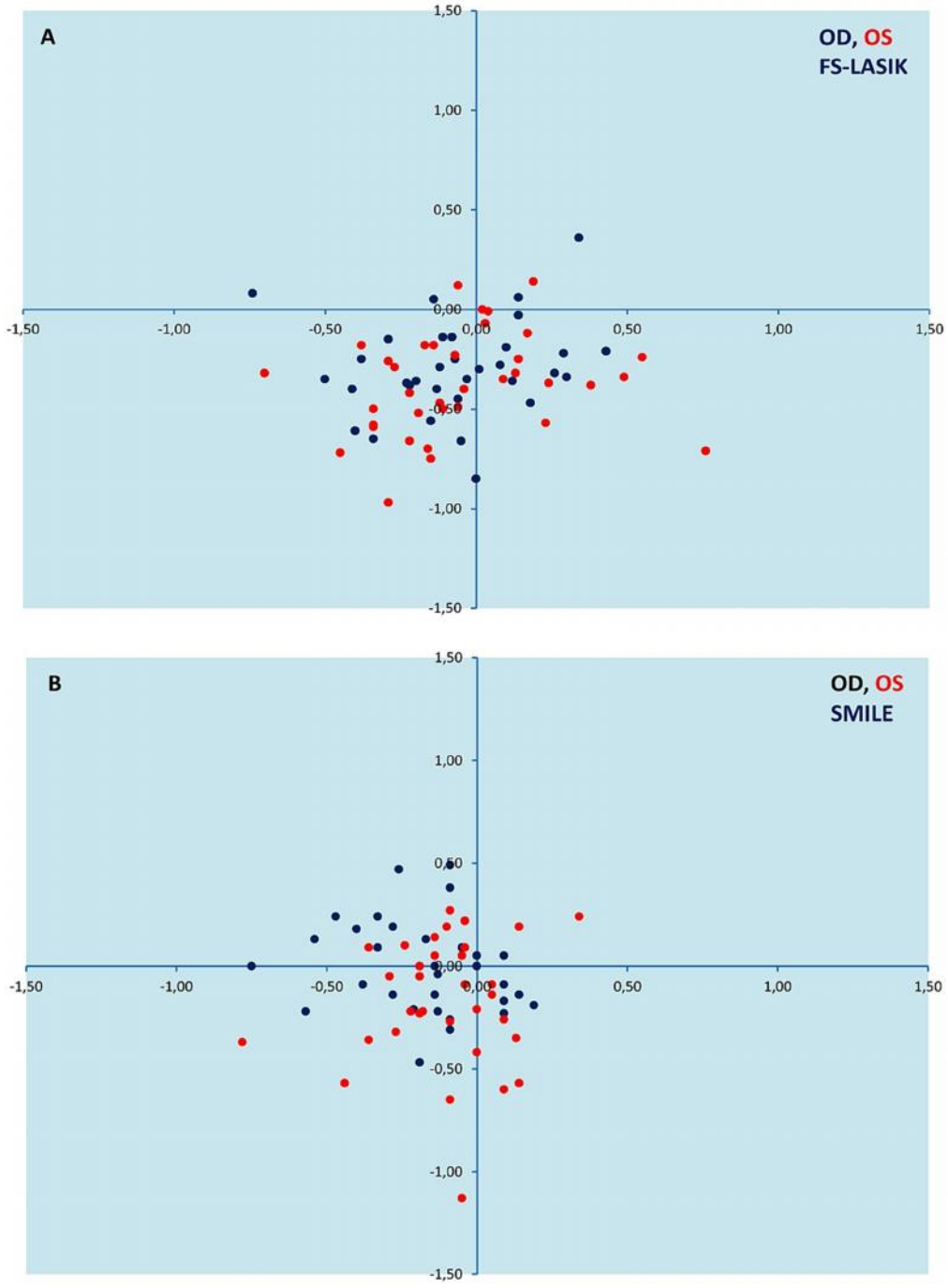

Fig. 12 (A) Achieved centration FS-LASIK group. Depiction of the PMPD in relation to the EPC (0,0). (B) Achieved centration in SMILE group. Depiction of the PMPD in relation to the preoperative CSCLR (0,0). Source [49, 52]

5.4 Analysis of the Pattern of the Achieved Centration

We estimated for both groups the pattern of the achieved centration in relation to the visual axis by depicting the PMPD of each eye in relation to the EPC (**Fig. 13A** and **13B**) and compared it to the preoperative pattern of the CSCLR in relation to the EPC. Then we examined for each eye the displacement of the PMPD in relation to the point corresponding to the preoperative CSCLR on the x-axis. The achieved centration would follow the pattern of angle K if the x-coordinate of the PMPD maintained the same sign (+ or -) as the x-coordinate of the preoperative CSCLR. We concluded that in SMILE group 52 out of 69 right eyes (75.36%) followed the pattern of angle K (**Fig. 10B** versus **Fig. 13B**), while in FS-LASIK group only 32 out of 69 (46.37%) followed that pattern ($P < 0.001$) (**Fig. 10A** versus **Fig. 13A**) (**Table 4**). As seen in **Fig. 13A**, the achieved centration in FS-LASIK in relation to the EPC (0,0) demonstrates a random distribution of the centre of the treatment zone of each patient. On the other hand, as seen in **Fig. 13B**, the achieved centration in SMILE group demonstrates a nasalisation pattern and a distribution that matches the pattern of angle K as presented in **Fig. 10B**.

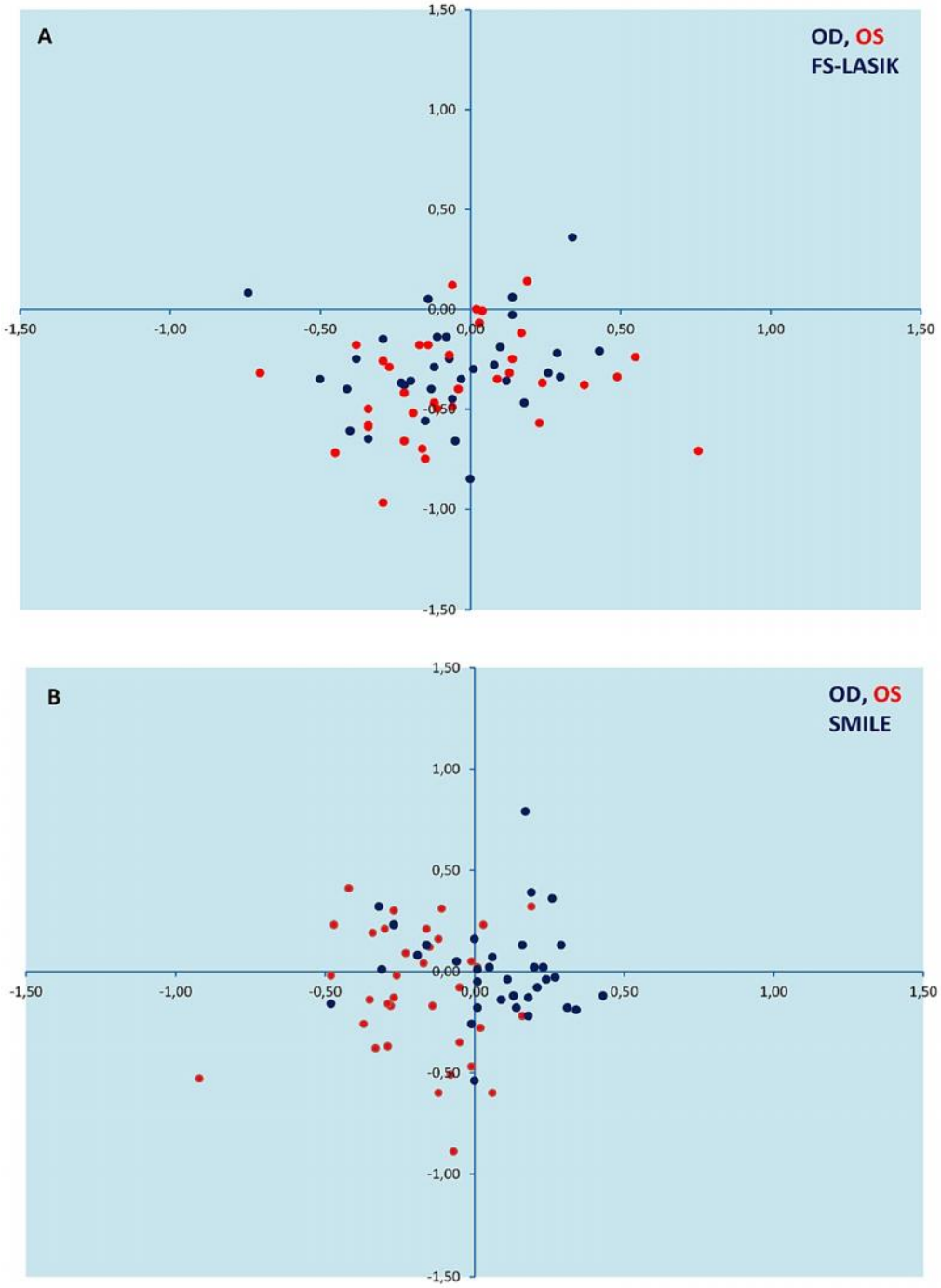

Fig. 13 Achieved centration in relation to the EPC (0,0). (A) FS-LASIK group. Random distribution of the centres of the treatment zone. (B) SMILE group. Distribution following the pattern of angle K. Source [49, 52]

Discussion

4.0 Methods of Centration Analysis

The estimation of the eccentricity of the treatment zone after refractive surgery is crucial in order to evaluate its visual impact and distinguish decentrations from pseudodecentrations, especially when attempting a retreatment. Refractive surgeons have previously attempted to estimate the extent of decentration by manipulating sheets of transparency film placed on the computer screen to point to the apparent centre of the treated area and measure its decentration [20]. Other groups proposed as a method of centration analysis the estimation of the intersecting point of the four farthest edges of the treatment zone in the x- and y-axis and defined the decentration as the distance of this point from the EPC [5, 59]. This approach, however, is according to our estimations not accurate because in cases of pseudodecentration or by peripheral abnormalities it does not point to the actual centre of the treatment zone. Many studies of centration analysis were based on subjective visual estimates by trained observers on topography maps, with most of them being conducted on tangential maps, axial maps or elevation maps [134]. An objective approach of centration analysis was presented by Qazi et al, using custom software on Orbscan topography in order to determine the topographic functional optical zone and the centroid of this zone on the refractive maps [93].

Before using the pachymetry maps for the centration analysis in our study, we also conducted the same measurements on tangential, axial and elevation differential maps. When the treatment zone was well centred, with well-defined edges, it was easy to visually identify its centroid on all these maps. However, in cases of sizable decentrations it was difficult to visually estimate the centre of the treatment zone on other maps rather than the pachymetry differential maps (**Fig. 14**). The pachymetry maps provide a very good depiction of the treatment zone and moreover, the centroid of this zone corresponds to the PMPD and therefore the centre of mass of the lenticule or the photoablated tissue, regardless of the extent of decentration.

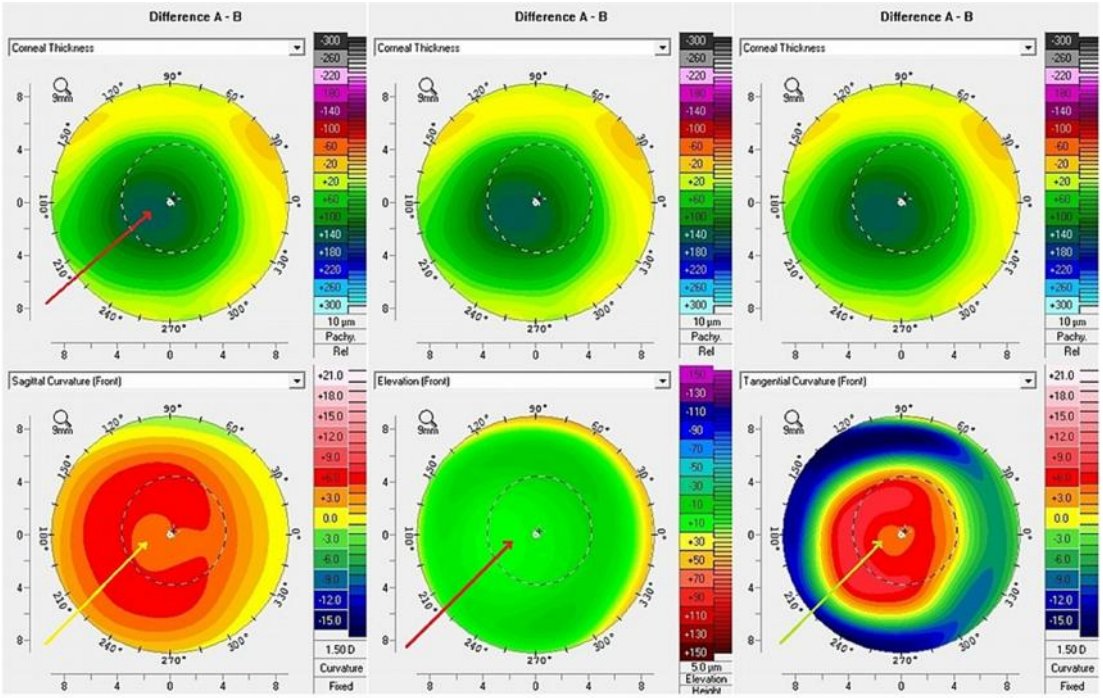

Fig. 14 SMILE case of extended decentration - Distance of the thickest point from CA: 0.863 mm. Distance of the thickest point from EPC: 1.062 mm. With the Pentacam software when we place the cursor at one point on the pachymetry maps we get the same point depicted on all other maps. Notice that a visual estimation of the centre of the treatment zone is easier on the differential pachymetry maps. The corneal thickness, as measured by Pentacam, is the distance between the anterior and posterior corneal surface, measured normal to the anterior surface tangent. This approach is commonly used for assessing the volume of the lenticule or the ablation and their spatial distribution in the corneal stroma. Moreover, the pachymetry maps despite being projected on a two-dimensional display, they provide sufficient three-dimensional data (pachymetry corresponds to the z-axis) and they generate reliable subtraction maps, provided that both pre- and postoperative measurements are well aligned. On the subtraction maps, the pachymetry progression from the periphery to the thickest point demonstrates the actual volume of the extracted lenticule or the photoablated tissue as well as its centre. Source [49, 52]

On the differential tangential maps, however, in cases of extended decentrations or peripheral abnormalities, the centre of the treatment zone was not that well depicted and moreover, in these cases the point of the maximum dioptre difference did not correspond to the centre of the treatment zone. According to the literature, the centre of the treatment zone on tangential differential maps is defined as the centroid of the area with a refractive power of 1.0 D more than the zero refractive power obtained from the differential map [74]. In our case, as demonstrated on **Fig. 14**, that would be the area inside the yellow-orange ring. A visual estimation of the centroid, in this case, is not as easy as on the pachymetry differential maps. The tangential maps would be the most appropriate maps to use in order to evaluate the refractive effect of decentration or estimate the degree of peripheral abnormalities [134]. The same problem is observed on the axial differential maps. In this case, the visual assessment of the centroid of the treatment zone is even more challenging due to the tendency of the axial algorithm to ignore minor variations in curvature. Visual estimations of the centre of the treatment zone on the differential elevation maps are also difficult since we cannot obtain good subtraction maps due to the resolution setting [134]. In a recent study, however, the researchers have used the postoperative elevation (front) map to analyse the centres of the optical zone, by setting the postoperative reference best-fit sphere (BFS) radius to have the same value as its preoperative counterpart [56].

A limitation of using pachymetry maps for our measurements is that, unlike curvature or elevation, corneal thickness is calculated normal to the anterior surface for most tomographic systems, including the Pentacam, and then reflected to a two-dimensional display. This leads to two main problems. First, the anterior surface is substantially altered after the refractive surgery and thus the normal-to-the-surface calculation and the direction, in which corneal thickness is calculated, are not comparable between preoperative and postoperative displays. Also, when potential misalignment exists between the preoperative and postoperative corneas relative to the reference axis (due to a change in the line of sight or other cause), the difference display can be adversely affected [105]. Moreover, subjective measurements always pose a human error factor. Therefore, it is necessary to introduce an objective method

of centration analysis, by using software for the various topography systems. Finally, the centration of 3-dimensional objects such as ablated areas or lenticules should be identified at 3 axes (x, y, z), therefore pointing the actual centre of mass and not only in 2 axes (x, y), therefore pointing the centroid of a surface [49].

Corneal thickness measured normal to the surface tangent might present value deviations compared to minimal distance measurements, especially when performed on an irregular (e.g. ectatic) cornea. Our examined groups included myopic, non-ectatic eyes that did not develop any iatrogenic ectasia (at least until the 3-month examination). Regarding our measurements, both the preoperative and postoperative measurements were performed with the same measurement principles and, despite the central corneal flattening after the surgery, they can be compared and subtracted. Corneal thickness maps may generate reliable subtraction maps, provided that each measurement is well aligned to the reference axis. In that case, the corneal thickness progression from the periphery to the thickest point demonstrates the volume of extracted lenticule or the photoablated tissue and its centre. Therefore, they provide sufficient three-dimensional data (corneal thickness corresponds to the z-axis), despite being projected on a two-dimensional display. Moreover, corneal refractive surgery causes a change of the corneal optics and the eye's visual optics, especially by decentered treatment zones. This is the reason that the predictability of the intraoperative alignment (coordinated in relation to the preoperative corneal parameters) was not assessed on the postoperative maps. Regarding the potential misalignment between preoperative and postoperative measurements, we relied on the quality specification data supplied by the instrument regarding the x, y, and z alignments, assuming that the algorithms used by the Pentacam to create subtraction maps would compensate for changes of the visual axis, the line of sight, or both, which are difficult (if not impossible) to determine accurately [53].

4.1 Subjective versus Objective Alignment

Standard ablation profiles and lenticule extractions can effectively correct myopic astigmatism. However, the quality of vision in many cases could decrease substantially, especially under mesopic and low contrast conditions, due to induction of HOA, even by subclinical decentrations as small as 0.2 mm [4, 68, 74]. The centration of a refractive procedure at the EPC allows the whole aperture of the eye's optical system to be covered with the ablation profile and minimizes the required optical zone [121]. In addition, the EPC can be easily located and tracked by eye tracking systems. This could potentially eliminate the risk of extended decentrations or non-homogenous ablation patterns. However, the pupil centre is an unstable point which shifts with changes in pupil diameter and the entrance pupil, used as reference point, is a virtual image of the real pupil as seen through the cornea [142].

Moreover, despite the technological advances of eye-tracking systems, the efficacy of the eye-trackers is well disputed in the literature with research groups showing no significant differences regarding moderate decentrations after myopic LASIK with or without eye-trackers. This could be explained by the fact that the majority of eye-trackers can follow the pupil in the x- and y-axes, with only the newest generation of eye trackers being able to detect cyclotorsional movements [24, 34]. In addition, the efficacy of pupil tracking might be limited due to parallax error since the eye tracker locates corneal positions by tracking the subjacent entrance pupil centre. Due to the parallax error changes of the fluence on the surface may occur when the eye rotates [13, 93].

On the other hand, the CSCLR provides a stable morphologic reference, which in cases of small angle K is considered a good approximation of the point where the visual axis intersects the cornea, offering, therefore, the opportunity of maintaining the functional corneal morphology after the surgery. Moreover, research groups showed no significant differences regarding the visual and refractive outcomes between corneal vertex and pupil centration. Nevertheless, less HOA were induced after centring the refractive procedure on the corneal vertex [4]. A problem that could arise by the centration on the CSCLR is that determining its exact location depends on the surgeon's

eye dominance, the surgeon's eye balance or the stereopsis angle of the microscope [4, 19].

Following the publication of the main outcomes presented in this dissertation [49], other research groups have examined the predictability of the intraoperative centration in SMILE and evaluated the effect of decentration on the postoperative quality of vision. Li et al. examined the decentration of the treatment zone on the postoperative elevation map (front), using the same radius value for the postoperative reference best-fit sphere as its preoperative counterpart. The decentration of the optical zone centre from the corneal vertex was measured 0.17 ± 0.09 mm, ranging from 0.02 to 0.49. Moreover, the decentration had in the majority of their cases a superior displacement. Out of the 100 measured eyes, there were 100 eyes within 0.50 mm (100%), 70 eyes within 0.20 mm (70%), and 90 eyes within 0.30 mm (90%) [56].

In a major comparative study between SMILE and eye-tracker based FS-LASIK, Reinstein et al. compared the optical zone centration accuracy between myopic eyes treated with the two techniques. In SMILE, the corneal vertex of the coaxially fixating eye was aligned with the vertex of the curved contact glass, and in FS-LASIK, the treatment was centred on the coaxially sighted corneal light reflex (first Purkinje image). The centration was evaluated on the tangential (instantaneous) curvature preoperative to postoperative difference map using a superimposed fixed grid and a set of concentric circles on the difference map to measure the offset between the optical zone centre and corneal vertex. The authors reported a mean centration offset of 0.20 ± 0.11 mm for SMILE and 0.17 ± 0.10 mm for the LASIK group, with no statistically significant difference between groups. In the same study, the optical zone in SMILE group was centred within 0.1 mm of the corneal vertex in 17% of eyes, within 0.2 mm in 55% of eyes, within 0.3 mm in 81% of eyes, and within 0.4 mm in 96% of eyes. In FS-LASIK group, the optical zone was centred within 0.1 mm of the corneal vertex in 24% of eyes, within 0.2 mm in 62% of eyes, within 0.3 mm in 92% of eyes, and within 0.4 mm in 98% of eyes [102].

In an attempt to evaluate the decentration of the optic zone after SMILE and its impact on visual and refractive outcomes, Liu et al. compared eyes according to the

displacement of the lenticule centre from the CV and EPC. The authors reported that the cases with the lenticule centre being closer to CV had better visual outcomes and less induced HOA compared to cases in which the lenticule centre was closer to EPC [61].

Yu et al. also evaluated and compared the decentration of the optical zone on elevation maps between eyes treated with SMILE and LASIK. According to their results, the mean decentration displacement in LASIK group was significantly more extended than in SMILE, without, however, significantly affecting the refractive and visual outcome [145].

In the most recent study regarding the intraoperative centration in SMILE by Wong et al., the authors evaluated the intraoperative decentration of the lenticule centre from the EPC and the CV using screen captures of intraoperative videos, obtained after suction and before the commencement of photodisruption. The authors reported a mean decentration from CV of 0.47 ± 0.25 mm, with 69.6% and 95.0% of eyes achieving a visual acuity of 20/20 and 20/30, respectively. The results also suggested a trend toward better efficacy in eyes which had decentered treatment from 0.4 to <0.6 mm from CV, while decentrations greater than 0.6 mm from CV may result in compromised visual outcomes. Finally, the authors recommended that patients with a large angle K, i.e. EPC to CV distance >0.6 mm, should have the lenticule created 0.4 to 0.6mm from the CV and not close to the EPC [138].

The results of our study as well as the results of many other centration studies that followed suggest that the argument of inferior centration outcomes in SMILE, due to the subjective alignment and lack of eye trackers, is not valid. On the contrary, according to our data (**Tables 4 & 5**), as well as the data from other studies, not only do we achieve a better centration in SMILE compared to LASIK but, moreover, the centration in the majority of cases follows the preoperative pattern of angle K, therefore resulting in a more natural centration closer to the visual axis. Furthermore, since the photodisruption is performed under suction, once we obtain a good centration, we can maintain it throughout the whole laser procedure without the need of intraoperative active eye tracking.

Conclusions

In summary, the present study showed that the pachymetry differential map in Scheimpflug based systems is a useful tool to display the treatment zone and to estimate the centration after refractive surgery. Regarding the achieved centration, our study showed that subjective alignment in SMILE had significantly better results compared to eye-tracker controlled alignment in FS-LASIK. Finally, according to our data, centring the refractive procedure on the CSCLR leads to a more natural centration outcome which follows the preoperative pattern of angle K, compared to centration on the EPC.

References

1. Abass A, Hayes S, White N, Sorensen T, Meek KM. Transverse depth-dependent changes in corneal collagen lamellar orientation and distribution. J R Soc Interface. 2015;12(104):20140717.
2. Alio JL, Rodriguez AE, Abdelghany AA, Oliveira RF. Autologous Platelet-Rich Plasma Eye Drops for the Treatment of Post-LASIK Chronic Ocular Surface Syndrome. J Ophthalmol. 2017;2017:2457620.
3. Arba-Mosquera S, Arbelaez MC. Three-month clinical outcomes with static and dynamic cyclotorsion correction using the SCHWIND AMARIS. Cornea. 2011;30(9):951-7.
4. Arbelaez MC, Vidal C, Arba-Mosquera S. Clinical outcomes of corneal vertex versus central pupil references with aberration-free ablation strategies and LASIK. Invest Ophthalmol Vis Sci. 2008;49(12):5287–5294.
5. Azar DT, Yeh PC. Corneal topographic evaluation of decentration in photorefractive keratektomy: treatment displacement vs intraoperative drift. Am J Ophthalmol. 1997;124(3):312-20.
6. Barraquer JI. Queratoplastia refractiva. Estudios Inform 1949;10:2–21.
7. Basmak H, Sahin A, Yildirim N, Papakostas TD, Kanellopoulos AJ. Measurement of angle kappa with synoptophore and Orbscan II in normal population. J Refract Surg. 2007;23(5):456–460.
8. Beuerman RW, Lemp MA. Tear Film. In: Mannis MJ, Holland EJ (Eds), *Cornea: Fundamentals, Diagnosis and Management.* 4th Edition. Elsevier Inc; 2017: pp. 32-39.
9. Bischoff M, Strobrawa G. Femtosecond Laser Keratomes for Small Incision Lenticule Extraction (SMILE). In: Sekundo W (Ed). *Small Incision Lenticule Extraction (SMILE): Principles, Techniques, Complication Management, and Future Concepts*. Springer International Publishing Switzerland; 2015: pp. 3-11.
10. Blum M, Sekundo W. Brief Historical Overview of the Clinical Development of ReLEx® Surgical Procedure. In: Sekundo W (Ed). *Small Incision Lenticule Extraction (SMILE): Principles, Techniques, Complication Management, and Future Concepts.* Springer International Publishing Switzerland; 2015: pp. 47-54.

11. Brissette-Storkus CS, Reynolds SM, Lepisto AJ, Hendricks RL. Identification of a novel macrophage population in the normal mouse corneal stroma. Invest Ophthalmol Vis Sci. 2002;43(7):2264-71.
12. Bruce AS, Brennan NA. Corneal pathophysiology with contact lens wear. Surv Ophthalmol. 1990;35(1):25-58. Review.
13. Bueeler M, Mrochen M. Limitations of pupil tracking in refractive surgery: systematic error in determination of corneal locations. J Refract Surg. 2004;20(4):371–378.
14. Bühren J, Yoon G, Kenner S, MacRae S, Huxlin K. The Effect of Optical Zone Decentration on Lower- and Higher-Order Aberrations after Photorefractive Keratectomy in a Cat Model. Invest Ophthalmol Vis Sci.. 2007;48(12):5806.
15. Chansue E. Current Technique and Instrumentation for SMILE. In: Sekundo W (Ed). *Small Incision Lenticule Extraction (SMILE): Principles, Techniques, Complication Management, and Future Concepts*. Springer International Publishing Switzerland; 2015: pp. 55-65.
16. Chen X, Wang Y, Zhang J, Yang S, Li X, Zhang L. Comparison of ocular higher-order aberrations after SMILE and Wavefront-guided Femtosecond LASIK for myopia. BMC Ophthalmology. 2017;17:42.
17. Ciccio AE, Durrie DS, Stahl JE, Schwendeman F. Ocular cyclotorsion during customized laser ablation. J Refract Surg. 2005;21(6):S772-4.
18. Conrady CD, Joos ZP, Patel BCK. Review: The Lacrimal Gland and Its Role in Dry Eye. J Ophthalmol. 2016; 2016:7542929.
19. de Ortueta D, Arba Mosquera S. Centration during hyperopic LASIK using the coaxial light reflex. J Refract Surg. 2007;23(1):11.
20. Deitz MR, Piebenga LW, Matta CS, Tauber J, Anello RD, DeLuca M. Ablation zone centration after photorefractive keratectomy and its effect on visual outcome. J Cataract Refract Surg. 1996;22(6):696-701.
21. Dong Z, Zhou X, Wu J, Zhang Z, Li T, Zhou Z, Zhang S, Li G. Small incision lenticule extraction (SMILE) and femtosecond laser LASIK: comparison of corneal wound healing and inflammation. Br J Ophthalmol. 2014;98(2):263-9.
22. Du Y, Funderburgh ML, Mann MM, SundarRaj N, Funderburgh JL. Multipotent Stem Cells in Human Corneal Stroma. Stem cells. 2005;23(9):1266-1275.

23. Dua HS, Faraj LA, Said DG, Gray T, Lowe J. Human corneal anatomy redefined: a novel pre-Descemet's layer (Dua's layer). Ophthalmology. 2013;120(9):1778-85.
24. El Bahrawy M, Alió JL. Excimer laser 6th generation: state of the art and refractive surgical outcomes. Eye and Vision. 2015;2:6.
25. Elkington AR, Frank HJ, Greaney MJ. Optics of Ametropia. In: Elkington AR, Frank HJ, Greaney MJ (Eds). *Clinical Optics,* 3rd Edition, Blackwell Science Ltd; 1999: pp. 113-140.
26. Elkington AR, Frank HJ, Greaney MJ. Refraction by the Eye. In: Elkington AR, Frank HJ, Greaney MJ (Eds). *Clinical Optics,* 3rd Edition, Blackwell Science Ltd; 1999: pp. 99-112.
27. Fay AM, Trokel SL, Myers JA. Pupil diameter and the principal ray. J Cataract Refract Surg. 1992;18(4):348-51.
28. Ganesh S, Brar S, Lazaridis A. Management and Outcomes of Retained Lenticules and Lenticule Fragments Removal After Failed Primary SMILE: A Case Series. J Refract Surg. 2017;33(12):848-853.
29. Ganesh S, Brar S, Pandey R, Pawar A. Interface healing and its correlation with visual recovery and quality of vision following small incision lenticule extraction. Indian J Ophthalmol 2018;66:212-8.
30. Ganesh S, Brar S, Pawar A. Results of Intraoperative Manual Cyclotorsion Compensation for Myopic Astigmatism in Patients Undergoing Small Incision Lenticule Extraction (SMILE). J Refract Surg. 2017;33(8):506-512.
31. Ganesh S, Brar S, Rao PA. Cryopreservation of extracted corneal lenticules after small incision lenticule extraction for potential use in human subjects. Cornea. 2014;33(12):1355-62.
32. Ganesh S, Gupta R. Comparison of visual and refractive outcomes following femtosecond laser- assisted lasik with smile in patients with myopia or myopic astigmatism. J Refract Surg. 2014;30(9):590-6.
33. Ganesh S. Refining Results with SMILE: Tips and Tricks. In: Sekundo W (Ed). *Small Incision Lenticule Extraction (SMILE): Principles, Techniques, Complication Management, and Future Concepts*. Springer International Publishing Switzerland; 2015: pp. 67-73.

34. Giaconi JA, Manche EE. Ablation centration in myopic laser in situ keratomileusis. Comparing the Visx S3 ActiveTrak and the Visx S2. J Cataract Refract Surg. 2003;29(8):1522-9.
35. Guarnieri FA. Corneal Biomechanics. In: Guarnieri FA (Ed.) *Corneal Biomechanics and Refractive Surgery*. Springer Science & Business Media New York; 2015: pp. 7-31.
36. Gyldenkerne A. Ivarsen A. Hjortdal JØ. Comparison of corneal shape changes and aberrations induced by FS-LASIK and SMILE for myopia. J Refract Surg. 2015;31(4):223-229.
37. Hjortdal JØ, Vestergaard AH, Ivarsen A, Ragunathan S, Asp S. Predictors for the outcome of small-incision lenticule extraction for Myopia. J Refract Surg. 2012;28(12):865-71.
38. Ivarsen A, Asp S, Hjortdal J. Safety and complications of more than 1500 small-incision lenticule extraction procedures. Ophthalmology. 2014;121(4):822-8.
39. Jacob S, Kumar DA, Agarwal A, Agarwal A, Aravind R, Saijimol AI. Preliminary Evidence of Successful Near Vision Enhancement With a New Technique: PrEsbyopic Allogenic Refractive Lenticule (PEARL) Corneal Inlay Using a SMILE Lenticule. J Refract Surg. 2017;33(4):224-229.
40. Kamiya K, Shimizu K, Ohmoto F. Comparison of the changes in corneal biomechanical properties after photorefractive keratectomy and laser in situ keratomileusis. Cornea. 2009;28(7):765-9.
41. Kanellopoulos AJ. Topography-Guided LASIK Versus Small Incision Lenticule Extraction (SMILE) for Myopia and Myopic Astigmatism: A Randomized, Prospective, Contralateral Eye Study. J Refract Surg. 2017 May 1;33(5):306-312.
42. Kardon R. Anatomy and Physiology of the Autonomic Nervous System. In: Miller NR, Newman NJ, Biousse V, Kerrison JB (Eds), *Walsh and Hoyt's Clinical Neuro-Ophthalmology,* 6th Edition. Lippincott Williams & Wilkins, Philadelphia; 2005: pp. 649-714.
43. Kermani O, Oberheide U, Schmiedt K, Gerten G, Bains HS. Outcomes of hyperopic LASIK with the NIDEK NAVEX platform centered on the visual axis or line of sight. J Refract Surg. 2009;25:98–103.

44. Khurana AK. Optics and Refraction. In: Khurana AK (Ed). *Comprehensive Ophthalmology,* 4th Edition, New Age International (P) Ltd., Publishers; 2007: pp. 19-49.
45. Kobashi H. Kamiya K. Shimizu K. Dry Eye After Small Incision Lenticule Extraction and Femtosecond Laser-Assisted LASIK: Meta-Analysis. Cornea. 2017;36(1):85-91.
46. Krueger RR, Trokel SL, Schubert HD. Interaction of ultraviolet laser light with the cornea. Invest Ophthalmol Vis Sci 1985;26:1455–1464.
47. Kymionis GD, Kankariya VP, Plaka AD, Reinstein DZ. Femtosecond laser technology in corneal refractive surgery: a review. J Refract Surg. 2012;28(12):912-20.
48. Lazaridis A, Droutsas K, Sekundo W, Petrak M, Schulze S. Corneal Clarity and Visual Outcomes after Small-Incision Lenticule Extraction and Comparison to Femtosecond Laser-Assisted In Situ Keratomileusis. J Ophthalmol. 2017;2017:5646390.
49. Lazaridis A, Droutsas K, Sekundo W. Topographic analysis of the centration of the treatment zone after SMILE for myopia and comparison to FS-LASIK: subjective versus objective alignment. J Refract Surg. 2014;30(10):680-6.
50. Lazaridis A, Messerschmidt-Roth A, Sekundo W, Schulze S. Refractive Lenticule Implantation for Correction of Ametropia: Case Reports and Literature Review. Klin Monbl Augenheilkd. 2017;234(1):77-89.
51. Lazaridis A, Reinstein DZ, Archer TJ, Schulze S, Sekundo W. Refractive Lenticule Transplantation for Correction of Iatrogenic Hyperopia and High Astigmatism After LASIK. J Refract Surg. 2016;32(11):780-786.
52. Lazaridis A, Sekundo W. Centration in SMILE for Myopia. In: Sekundo W (Ed). *Small Incision Lenticule Extraction (SMILE): Principles, Techniques, Complication Management, and Future Concepts*. Springer International Publishing Switzerland; 2015: pp. 143-156.
53. Lazaridis A. Error in the estimation of ablation centration using pachymetric difference maps. J Refract Surg. 2015;31(2):139.
54. Lee YC. Active eye-tracking improves LASIK results. J Refract Surg. 2007;23(6):581-5.

55. Leonardi A, Tavolato M, Curnow SJ, Fregona IA, Violato D, Alió JL. Cytokine and chemokine levels in tears and in corneal fibroblast cultures before and after excimer laser treatment. J Cataract Refract Surg. 2009;35(2):240-7.
56. Li M, Zhao J, Miao H, Shen Y, Sun L, Tian M, Wadium E, Zhou X. Mild decentration measured by a Scheimpflug camera and its impact on visual quality following SMILE in the early learning curve. Invest Ophthalmol Vis Sci. 2014;55(6):3886-92.
57. Li X, Wang Y, Dou R. Aberration compensation between anterior and posterior corneal surfaces after Small incision lenticule extraction and Femtosecond laser-assisted laser in-situ keratomileusis. Ophthalmic Physiol Opt. 2015;35(5):540-51.
58. Liang G, Chen X, Zha X, Zhang F. A Nomogram to Improve Predictability of Small-Incision Lenticule Extraction Surgery. Med Sci Mon Int Med J Exp Clin Res. 2017;23:5168-5175.
59. Lin DT, Sutton HF, Berman M. Corneal topography following excimer photorefractive keratectomy for myopia. J Cataract Refract Surg. 1993;19 Suppl:149-54.
60. Lin F, Xu Y, Yang Y. Comparison of the visual results after SMILE and femtosecond laser-assisted LASIK for myopia. J Refract Surg. 2014;30(4):248-54.
61. Liu M, Sun Y, Wang D, Zhang T, Zhou Y, Zheng H, Liu Q. Decentration of optical zone center and its impact on visual outcomes following SMILE. Cornea. 2015;34(4):392-7.
62. Liu M, Wang J, Zhong W, Wang D, Zhou Y, Liu Q. Impact of Suction Loss During Small Incision Lenticule Extraction (SMILE). J Refract Surg. 2016;32(10):686-692.
63. Liu YC, Ang HP, Teo EP, Lwin NC, Yam GH, Mehta JS. Wound healing profiles of hyperopic-small incision lenticule extraction (SMILE). Sci Rep. 2016;6:29802.
64. Liu YC, Tan DTH , Mehta JS. Wound Healing After ReLEx® Surgery. In: Sekundo W (Ed). *Small Incision Lenticule Extraction (SMILE): Principles, Techniques, Complication Management, and Future Concepts.* Springer International Publishing Switzerland; 2015: pp. 13-25.

65. Liu YC, Teo EPW, Ang HP, Seah XY, Lwin NC, Yam GHF, Mehta JS. Biological corneal inlay for presbyopia derived from small incision lenticule extraction (SMILE). Sci Rep. 2018;8(1):1831.
66. Mandell RB, Chiang CS, Klein SA. Location of the major corneal reference points. Optom Vis Sci. 1995;72(11):776-84.
67. Mastropasqua L, Nubile M. Corneal Nerve and Keratocyte Response to ReLEx® Surgery. In: Sekundo W (Ed). *Small Incision Lenticule Extraction (SMILE): Principles, Techniques, Complication Management, and Future Concepts.* Springer International Publishing Switzerland; 2015: pp. 27-42.
68. Mastropasqua L, Toto L, Zuppardi E, Nubile M, Carpineto P, Di Nicola M, Ballone E. Photorefractive keratectomy with aspheric profi le of ablation versus conventional photorefractive keratectomy for myopia correction: six-month controlled clinical trial. J Cataract Refract Surg. 2006;32(1):109–116.
69. McAlinden C. Corneal refractive surgery: past to present. Clin Exp Optom. 2012;95(4):386-98.
70. Melki SA, Azar DT. LASIK complications: etiology, management, and prevention. Surv Ophthalmol. 2001;46(2):95-116.
71. Messerschmidt-Roth A, Sekundo W, Lazaridis A, Schulze S. Three Years Follow-up Study after Refractive Small Incision Lenticule Extraction (SMILE) Using 500 kHz Femtosecond Laser in "Fast Mode". Klin Monbl Augenheilkd. 2017; 234(1):102-108.
72. Mohamed-Noriega K, Mehta JS. Femtosecond Refractive Lenticule Extraction and Small Incision Lenticule Extraction. In: Copeland RA, Afshari NA (Eds). *Copeland and Afshari's Principles and Practice of Cornea.* Jaypee Brothers Medical Publishers; 2013: pp. 1405-1420.
73. Moshirfar M, Albarracin JC, Desautels JD, Birdsong OC, Linn SH, Hoopes PC Sr. Ectasia following small-incision lenticule extraction (SMILE): a review of the literature. Clin Ophthalmol. 2017;11:1683-1688.
74. Mrochen M, Kaemmerer M, Mierdel P, Seiler T. Increased higher-order optical aberrations after laser refractive surgery: a problem of subclinical decentration. J Cataract Refract Surg. 2001;27(3):362–369.

75. Mulhern MG, Foley-Nolan A, O'Keefe M, Condon PI. Topographical analysis of ablation centration after excimer laser photorefractive keratectomy and laser in situ keratomileusis for high myopia. J Cataract Refract Surg. 1997;23(4):488–494.
76. Müller B, Boeck T, Hartmann C. Effect of excimer laser beam delivery and beam shaping on corneal sphericity in photorefractive keratectomy. J Cataract Refract Surg. 2004;30(2):464-70.
77. Munnerlyn CR, Koons SJ, Marshall J. Photorefractive keratectomy: a technique for laser refractive surgery. J Cataract Refract Surg. 1988;14(1):46-52.
78. Neuhann IM, Lege BA, Bauer M, Hassel JM, Hilger A, Neuhann TF. Static and dynamic rotational eye tracking during LASIK treatment of myopic astigmatism with the Zyoptix laser platform and Advanced Control Eye Tracker. J Refract Surg. 2010;26(1):17-27.
79. Ní Dhubhghaill S, Rozema JJ, Jongenelen S, Ruiz Hidalgo I, Zakaria N, Tassignon MJ. Normative values for corneal densitometry analysis by Scheimpflug optical assessment. Invest Ophthalmol Vis Sci. 2014;55(1):162-8.
80. Nichols KK, Foulks GN, Bron AJ, Glasgow BJ, Dogru M, Tsubota K, Lemp MA, Sullivan DA. The International Workshop on Meibomian Gland Dysfunction: Executive Summary. Invest Ophthalmol Vis Sci. 2011;52(4):1922-1929.
81. Nishida T, Saika S, Morishige N. Cornea and Sclera: Anatomy and Physiology. In: Mannis MJ, Holland EJ (Eds), *Cornea: Fundamentals, Diagnosis and Management.* 4th Edition. Elsevier Inc; 2017: pp. 1-22.
82. Nishida T, Saika S. Cornea and Sclera: Anatomy and Physiology. In: Krachmer JH, Mannis MJ, Holland EJ (Eds), *Cornea: Fundamentals, Diagnosis and Management*. 3rd Edition. Mosby; 2011: pp. 3-24.
83. Pajic B, Cvejic Z, Mijatovic Z, Indjin D, Mueller J. Excimer Laser Surgery: Biometrical Iris Eye Recognition with Cyclorotational Control Eye Tracker System. Sensors (Basel). 2017;17(6). pii: E1211.
84. Pajic B, Vastardis I, Pajic-Eggspuehler B, Gatzioufas Z, Hafezi F. Femtosecond laser versus mechanical microkeratome-assisted flap creation for LASIK: a prospective, randomized, paired-eye study. Clin Ophthalmol. 2014;8:1883-9.

85. Pallikaris I, Papadaki T. History of LASIK. In Azar DT, Koch DD (Eds). *LASIK: Fundamentals, Surgical Techniques, and Complications.* Marcel Dekker, Inc; 2002: pp. 21-38.
86. Pallikaris IG, Kymionis GD, Panagopoulou SI, Siganos CS, Theodorakis MA, Pallikaris AI. Induced optical aberrations following formation of a laser in situ keratomileusis flap. J Cataract Refract Surg. 2002;28(10):1737-41.
87. Pallikaris IG, Papatzanaki ME, Siganos DS, Tsilimbaris MK. A corneal flap technique for laser in situ keratomileusis. Human studies. Arch Ophthalmol. 1991;109(12):1699-702.
88. Pallikaris IG, Papatzanaki ME, Stathi EZ, Frenschock O, Georgiadis A. Laser in situ keratomileusis. Lasers Surg Med. 1990;10(5):463-8.
89. Pande M, Hillman JS. Optical zone centration in keratorefractive surgery. Entrance pupil center, visual axis, coaxially sighted corneal reflex, or geometric corneal center? Ophthalmology. 1993;100(8):1230-7.
90. Park CY, Oh SY, Chuck RS. Measurement of angle kappa and centration in refractive surgery. Curr Opin Ophthalmol. 2012;23(4):269–275.
91. Pietilä J, Huhtala A, Mäkinen P, Uusitalo H. Flap characteristics, predictability, and safety of the Ziemer FEMTO LDV femtosecond laser with the disposable suction ring for LASIK. Eye (Lond). 2014;28(1):66-71.
92. Podskochy A. Protective role of corneal epithelium against ultraviolet radiation damage. Acta Ophthalmol Scand. 2004;82(6):714-7.
93. Qazi MA, Pepose JS, Sanderson JP, Mahmoud AM, Roberts CJ. Novel objective method for comparing ablation centration with and without pupil tracking following myopic laser in situ keratomileusis using the bausch & lomb technolas 217A. Cornea. 2009;28(6):616–625.
94. Randleman JB, Dawson DG, Grossniklaus HE, McCarey BE, Edelhauser HF. Depth-dependent cohesive tensile strength in human donor corneas: implications for refractive surgery. J Refract Surg. 2008;24(1):S85-9.
95. Randleman JB, Shah RD. LASIK Interface Complications: Etiology, Management, & Outcomes. J Refract Surg. 2012;28(8):575-586.

96. Randleman JB, Trattler WB, Stulting RD. Validation of the Ectasia Risk Score System for preoperative laser in situ keratomileusis screening. Am J Ophthalmol. 2008;145(5):813-8.
97. Ratkay-Traub I, Ferincz IE, Juhasz T, Kurtz RM, Krueger RR. First clinical results with the femtosecond neodynium-glass laser in refractive surgery. J Refract Surg. 2003;19(2):94-103.
98. Reinstein DZ, Archer TJ, Gobbe M, Silverman RH, Coleman DJ. Epithelial thickness in the normal cornea: three-dimensional display with Artemis very high-frequency digital ultrasound. J Refract Surg. 2008;24(6):571-81.
99. Reinstein DZ, Archer TJ, Randleman JB. Mathematical model to compare the relative tensile strength of the cornea after PRK, LASIK, and small incision lenticule extraction. J Refract Surg. 2013;29(7):454-60.
100. Reinstein DZ, Carp GI, Archer TJ, Gobbe M. Outcomes of small incision lenticule extraction (SMILE) in low myopia. J Refract Surg. 2014;30(12):812-8.
101. Reinstein DZ, Gobbe M, Archer TJ. Coaxially sighted corneal light reflex versus entrance pupil center centration of moderate to high hyperopic corneal ablations in eyes with small and large angle kappa. J Refract Surg. 2013;29(8):518-25.
102. Reinstein DZ, Gobbe M, Gobbe L, Archer TJ, Carp GI. Optical Zone Centration Accuracy Using Corneal Fixation-based SMILE Compared to Eye Tracker-based Femtosecond Laser-assisted LASIK for Myopia. J Refract Surg. 2015;31(9):586-92.
103. Reinstein DZ. Why I Chose My Excimer Laser Platform. CRSTEurope website. https://crstodayeurope.com/articles/2013-julaug/why-i-chose-my-excimer-laser-platform/. Accessed July 28, 2018.
104. Riau AK, Angunawela RI, Chaurasia SS, Lee WS, Tan DT, Mehta JS. Early corneal wound healing and inflammatory responses after refractive lenticule extraction (ReLEx). Invest Ophthalmol Vis Sci. 2011;52(9):6213-21.
105. Roberts CJ. Error in the estimation of ablation centration using pachymetric difference maps. J Refract Surg. 2015;31(2):138-9.
106. Roque MR, Melki SA, Azar DT, Yeung EY. Management of Flap Complications in LASIK. In Azar DT, Koch DD (Eds). *LASIK: Fundamentals, Surgical Techniques, and Complications.* Marcel Dekker, Inc; 2002: pp. 431-462.

107. Rosenfield M. Refractive Status of the Eye. In: Benjamin WJ (Ed). *Borish's Clinical Refraction*, 2nd Edition, Elsevier Inc. 2006: pp. 3-34.
108. Santhiago MR, Giacomin NT, Smadja D, Bechara SJ. Ectasia risk factors in refractive surgery. Clin Ophthalmol. 2016;10:713-720.
109. Scott WE, Mash AJ. Kappa angle measures of strabismic and nonstrabismic individuals. Arch Ophthalmol. 1973;89(1):18–20.
110. Sekundo W, Gertnere J, Bertelmann T, Solomatin I. One-year refractive results, contrast sensitivity, high-order aberrations and complications after myopic small-incision lenticule extraction (ReLEx SMILE). Graefes Arch Clin Exp Ophthalmol. 2014;252(5):837-843.
111. Sekundo W, Kunert K, Russmann C, Gille A, Bissmann W, Stobrawa G, Sticker M, Bischoff M, Blum M. First efficacy and safety study of femtosecond lenticule extraction for the correction of myopia: six-month results. J Cataract Refract Surg. 2008;34(9):1513-20.
112. Sekundo W, Kunert KS, Blum M. Small incision corneal refractive surgery using the small incision lenticule extraction (SMILE) procedure for the correction of myopia and myopic astigmatism: results of a 6 month prospective study. Br J Ophthalmol. 2011;95(3):335-9.
113. Shah R. Complications After SMILE and Its Management Including Re-treatment Techniques. In: Sekundo W (Ed). *Small Incision Lenticule Extraction (SMILE): Principles, Techniques, Complication Management, and Future Concepts*. Springer International Publishing Switzerland; 2015: pp. 97-105.
114. Shortt AJ, Allan BD, Evans JR. Laser-assisted in-situ keratomileusis (LASIK) versus photorefractive keratectomy (PRK) for myopia. Cochrane Database Syst Rev. 2013;(1):CD005135.
115. Shtein RM. Post-LASIK dry eye. Expert Rev Ophthalmol. 2011;6(5):575-582.
116. Sinjab MM. Corneal Thickness Map and Relative Thickness Map. In: Sinjab MM (Ed). *Corneal Topography in Clinical Practice (Pentacam System): Basics and Clinical Interpretation,* 2nd Edition, Jaypee Brothers Medical Publishers; 2012: pp. 52-59.

117. Sinjab MM. Curvature Maps / Corneal Power Maps. In: Sinjab MM (Ed). *Corneal Topography in Clinical Practice (Pentacam System): Basics and Clinical Interpretation,* 2nd Edition, Jaypee Brothers Medical Publishers; 2012: pp. 16-37.

118. Sinjab MM. Elevation Maps. In: Sinjab MM (Ed). *Corneal Topography in Clinical Practice (Pentacam System): Basics and Clinical Interpretation,* 2nd Edition, Jaypee Brothers Medical Publishers; 2012: pp. 40-50.

119. Sinjab MM. Instruments to Measure the Corneal Surface. In: Sinjab MM (Ed). *Corneal Topography in Clinical Practice (Pentacam System): Basics and Clinical Interpretation,* 2nd Edition, Jaypee Brothers Medical Publishers; 2012: pp. 7-12.

120. Skalicky SE. Protective Mechanisms of the Eye and the Eyelids. In: Skalicky SE (Ed) *Ocular and Visual Physiology,* Springer Science+Business Media Singapore; 2016: pp. 3-12.

121. Soler V, Benito A, Soler P, Triozon C, Arné JL, Madariaga V, Artal P, Malecaze F. A randomized comparison of pupil-centered versus vertex-centered ablation in LASIK correction of hyperopia. Am J Ophthalmol. 201;152(4):591-599.

122. Spiru B, Kling S, Hafezi F, Sekundo W. Biomechanical Differences Between Femtosecond Lenticule Extraction (FLEx) and Small Incision Lenticule Extraction (SMILE) Tested by 2D-Extensometry in Ex Vivo Porcine Eyes. Invest Ophthalmol Vis Sci. 2017;58(5):2591-2595.

123. Srivannaboon S, Reinstein DZ, Archer TJ, Chansue E. Spherical aberration from myopic excimer laser ablation for aspheric and non-aspheric profiles. Optom Vis Sci. 2012;89(8):1211-8.

124. Sutton G, Hodge C. Accuracy and precision of LASIK flap thickness using the IntraLase femtosecond laser in 1000 consecutive cases. J Refract Surg. 2008;24(8):802-6.

125. Tabernero J, Benito A, Alcon E, Artal P. Mechanism of compensation of aberrations in the human eye. J Opt Soc Am A Opt Image Sci Vis. 2007;24(10):3274–3283.

126. Talamo JH, Meltzer J, Gardner J. Reproducibility of flap thickness with IntraLase FS and Moria LSK-1 and M2 microkeratomes. J Refract Surg. 2006;22(6):556-61.

127. Taylor NM, Eikelboom RH, van Sarloos PP, Reid PG. Determining the accuracy of an eye tracking system for laser refractive surgery. J Refract Surg. 2000;16(5):S643-6.
128. Terrell J, Bechara SJ, Nesburn A, Waring GO, Macy J, Maloney RK. The effect of globe fixation on ablation zone centration in photorefractive keratectomy. Am J Ophthalmol. 1995;119(5):612–619.
129. Theophanous C, Jacobs DS, Hamrah P. Corneal Neuralgia after LASIK. Optom Vis Sci. 2015;92(9):e233-40.
130. Torres R, Ang RT, Azar DT. Lasers in LASIK: Basic Aspects. In Azar DT, Koch DD (Eds). *LASIK: Fundamentals, Surgical Techniques, and Complications*. Marcel Dekker, Inc; 2002: pp. 39-56.
131. Tsai YY, Lin JM. Ablation centration after active eye-tracker-assisted photorefractive keratectomy and laser in situ keratomileusis. J Cataract Refract Surg. 2000;26(1):28-34.
132. Uozato H, Guyton DL. Centering corneal surgical procedures. Am J Ophthalmol. 1987;103:264-75.
133. Villavicencio O, Belin MW, Ambrósio R Jr, Steinmueller A. Corneal pachymetry: new ways to look at an old measurement. J Cataract Refract Surg. 2014;40(5):695-701.
134. Vinciguerra P, Randazzo A, Albè E, Epstein D. Tangential topography corneal map to diagnose laser treatment decentration. J Refract Surg. 2007;23(9 Suppl):S1057-64.
135. Von Noorden GK, Campos EC. Examination of the patient II. In: *Binocular vision and ocular motility-theory and management of strabismus*, 6th Edition. Mosby, St. Louis; 2002: pp. 168–210.
136. Wang D, Liu M, Chen Y, Zhang X, Xu Y, Wang J, To CH, Liu Q. Differences in the corneal biomechanical changes after SMILE and LASIK. J Refract Surg. 2014;30(10):702-707.
137. West-Mays JA, Dwivedi DJ. The keratocyte: corneal stromal cell with variable repair phenotypes. Int J Biochem Cell Biol. 2006;38(10):1625-31.
138. Wong JX, Wong EP, Htoon HM, Mehta JS. Intraoperative centration during small incision lenticule extraction (SMILE). Medicine (Baltimore). 2017;96(16):e6076.

139. Xu J, Bao J, Lu F, He JC. An indirect method to compare the reference centres for corneal measurements. Ophthalmic Physiol Opt. 2012;32(2):125-32.
140. Yan H, Gong LY, Huang W, Peng YL. Clinical outcomes of small incision lenticule extraction versus femtosecond laser-assisted LASIK for myopia: a Meta-analysis. Int J Ophthalmol. 2017;10(9):1436-1445.
141. Yang E, Roberts CJ, Mehta JS. A Review of Corneal Biomechanics after LASIK and SMILE and the Current Methods of Corneal Biomechanical Analysis. J Clin Exp Ophthalmol. 2015;6:507.
142. Yang Y, Thompson K, Burns S. Pupil location under mesopic, photopic and pharmacologically dilated conditions. Invest Ophthalmol Vis Sci. 2002;43(7):2508–2512.
143. Ye M, Liu C, Liao R, Gu Z, Zhao B, Liao Y. SMILE and Wavefront-Guided LASIK Out-Compete Other Refractive Surgeries in Ameliorating the Induction of High-Order Aberrations in Anterior Corneal Surface. J Ophthalmol. 2016;2016:8702162.
144. Yoon JJ, Ismail S, Sherwin T. Limbal stem cells: Central concepts of corneal epithelial homeostasis. World J Stem Cells. 2014;6(4):391-403.
145. Yu Y, Zhang W, Cheng X, Cai J, Chen H. Impact of Treatment Decentration on Higher-Order Aberrations after SMILE. J Ophthalmol. 2017;2017:9575723.

Acknowledgements

I would like to show my gratitude to Professor Walter Sekundo, director of the University Eye Clinic of Marburg, for sharing his pearls of wisdom and expertise with me during the course of this research and afterwards. The time he invested and the knowledge he shared, enabled the completion of my dissertation thesis, as well as many other studies that followed. His effort and contribution are highly appreciated. I wish him every happiness and success in his personal life and academic career.

I would also like to thank my parents, Magda and Andreas, for their love and all their contributions and support, as well as my aunt, Niki, for loving, supporting and motivating me throughout my life.

I would like to thank my brother, Savvas, for his support and love as well as his assistance in editing all the graphs and figures in this dissertation thesis and many other publications.

I would like to thank my friends for all the experiences and laughter we shared together, and for being there for me in good and hard moments.

Above all, I would like to thank my girlfriend, Stavroula, for her unconditional love, care, advice and support. She is and has always been my guardian angel, my greatest love and inspiration.

Declaration of Honour Regarding the Autonomous Preparation of Dissertation Thesis

"I declare on my honour that I have submitted the dissertation entitled „Topographic analysis of the centration of the treatment zone after Small Incision Lenticule Extraction (SMILE) surgery for myopia and myopic astigmatism and comparison to Femtosecond laser-assisted LASIK (FS-LASIK)“ to the Department of Medicine, University of Marburg, for doctoral examination. The dissertation was completed at the Department of Ophthalmology of the University of Marburg, under the supervision and support of the director of the Department, Professor Walter Sekundo.

I have prepared the present work independently, without receiving any help or assistance for its completion. I did not use any other resources for drafting the thesis than those listed in the dissertation. I have neither submitted an application for admission to a doctorate at any other German or foreign medical department nor have I submitted the present or any other dissertation elsewhere.

I assure you that verbatim or non-verbatim citations are all marked and their origin is specified. This also applies to figures and illustrations, as well as to online sources. I agree with the use of software for the detection of plagiarism. Additionally, I declare that the digital version submitted matches invariably the printed version in content and wording.

The present work was published in the following publications:

1. Lazaridis A, Droutsas K, Sekundo W. Topographic analysis of the centration of the treatment zone after SMILE for myopia and comparison to FS-LASIK: subjective versus objective alignment. J Refract Surg. 2014;30(10):680-6.
2. Lazaridis A, Sekundo W. Centration in SMILE for Myopia. In: Sekundo W (Ed). *Small Incision Lenticule Extraction (SMILE): Principles, Techniques, Complication Management, and Future Concepts*. Springer International Publishing Switzerland; 2015: pp. 143-156.
3. Lazaridis A, Droutsas K, Sekundo W, Petrak M, Schulze S. Corneal Clarity and Visual Outcomes after Small-Incision Lenticule Extraction and Comparison to

Femtosecond Laser-Assisted In Situ Keratomileusis. J Ophthalmol. 2017;2017:5646390.

4. Messerschmidt-Roth A, Sekundo W, Lazaridis A, Schulze S. Three Years Follow-up Study after Refractive Small Incision Lenticule Extraction (SMILE) Using 500 kHz Femtosecond Laser in "Fast Mode". Klin Monbl Augenheilkd. 2017; 234(1):102-108.
5. Lazaridis A. Error in the estimation of ablation centration using pachymetric difference maps. J Refract Surg. 2015;31(2):139.
6. Lazaridis A, Messerschmidt-Roth A, Sekundo W, Schulze S. Refractive Lenticule Implantation for Correction of Ametropia: Case Reports and Literature Review. Klin Monbl Augenheilkd. 2017;234(1):77-89.
7. Lazaridis A, Reinstein DZ, Archer TJ, Schulze S, Sekundo W. Refractive Lenticule Transplantation for Correction of Iatrogenic Hyperopia and High Astigmatism After LASIK. J Refract Surg. 2016;32(11):780-786.
8. Ganesh S, Brar S, Lazaridis A. Management and Outcomes of Retained Lenticules and Lenticule Fragments Removal After Failed Primary SMILE: A Case Series. J Refract Surg. 2017;33(12):848-853.

Marburg, 28.07.2018, Signature

I have taken note of the instructions for the detection of plagiarism.

Marburg, 28.07.2018, Signature of Supervisor“

Ehrenwörtliche Erklärung über die selbstständige Anfertigung der Dissertation

„Ich erkläre ehrenwörtlich, dass ich die dem Fachbereich Medizin Marburg zur Promotionsprüfung eingereichte Arbeit mit dem Titel „Topographic analysis of the centration of the treatment zone after Small Incision Lenticule Extraction (SMILE) surgery for myopia and myopic astigmatism and comparison to Femtosecond laser-assisted LASIK (FS-LASIK)“, in der Klinik für Audenheilkunde unter Leitung und mit Unterstützung von Professor Dr. med. Walter Sekundo, ohne sonstige Hilfe selbst durchgeführt und bei der Abfassung der Arbeit keine anderen als die in der Dissertation aufgeführten Hilfsmittel benutzt habe. Ich habe bisher an keinem in- oder ausländischen Medizinischen Fachbereich ein Gesuch um Zulassung zur Promotion eingereicht, noch die vorliegende oder eine andere Arbeit als Dissertation vorgelegt. Ich versichere, dass ich sämtliche wörtlichen oder sinngemäßen Übernahmen und Zitate kenntlich gemacht habe. Mit dem Einsatz von Software zur Erkennung von Plagiaten bin ich einverstanden. Vorliegende Arbeit wurde in folgenden Publikationsorganen veröffentlicht:

1. Lazaridis A, Droutsas K, Sekundo W. Topographic analysis of the centration of the treatment zone after SMILE for myopia and comparison to FS-LASIK: subjective versus objective alignment. J Refract Surg. 2014;30(10):680-6.
2. Lazaridis A, Sekundo W. Centration in SMILE for Myopia. In: Sekundo W (Ed). *Small Incision Lenticule Extraction (SMILE): Principles, Techniques, Complication Management, and Future Concepts*. Springer International Publishing Switzerland; 2015: pp. 143-156.
3. Lazaridis A, Droutsas K, Sekundo W, Petrak M, Schulze S. Corneal Clarity and Visual Outcomes after Small-Incision Lenticule Extraction and Comparison to Femtosecond Laser-Assisted In Situ Keratomileusis. J Ophthalmol. 2017;2017:5646390.
4. Messerschmidt-Roth A, Sekundo W, Lazaridis A, Schulze S. Three Years Follow-up Study after Refractive Small Incision Lenticule Extraction (SMILE)

Using 500 kHz Femtosecond Laser in "Fast Mode". Klin Monbl Augenheilkd. 2017;234(1):102-108.

5. Lazaridis A. Error in the estimation of ablation centration using pachymetric difference maps. J Refract Surg. 2015;31(2):139.
6. Lazaridis A, Messerschmidt-Roth A, Sekundo W, Schulze S. Refractive Lenticule Implantation for Correction of Ametropia: Case Reports and Literature Review. Klin Monbl Augenheilkd. 2017;234(1):77-89.
7. Lazaridis A, Reinstein DZ, Archer TJ, Schulze S, Sekundo W. Refractive Lenticule Transplantation for Correction of Iatrogenic Hyperopia and High Astigmatism After LASIK. J Refract Surg. 2016;32(11):780-786.
8. Ganesh S, Brar S, Lazaridis A. Management and Outcomes of Retained Lenticules and Lenticule Fragments Removal After Failed Primary SMILE: A Case Series. J Refract Surg. 2017;33(12):848-853.

Marburg, 28.07.2018, Unterschrift

Die Hinweise zur Erkennung von Plagiaten habe ich zur Kenntnis genommen.

Marburg, 28.07.2018, Unterschrift Betreuer